

# Estimation of elastic seismic demands in TU structures using interactive relations between shear and torsion

Ruth A. Abegaz<sup>a</sup> and Han Seon Lee\*

School of Civil, Environmental, and Architectural Engineering, Korea University, Seoul, 02841 Republic of Korea

(Received February 19, 2020, Revised June 9, 2020, Accepted July, 14, 2020)

**Abstract.** The code static eccentricity model for elastic torsional design of structures has two critical shortcomings: (1) the negation of the inertial torsional moment at the center of mass (CM), particularly for torsionally-unbalanced (TU) building structures, and (2) the confusion caused by the discrepancy in the definition of the design eccentricity in codes and the resistance eccentricity commonly used by engineers such as in FEMA454. To overcome these shortcomings, using the resistance eccentricity model that can accommodate the inertial torsional moment at the CM, interactive relations between shear and torsion are proposed as follows: (1) elastic responses of structures at instants of peak edge-frame drifts are given as functions of resistance eccentricity, and (2) elastic hysteretic relationships between shear and torsion in forces and deformations are bounded by ellipsoids constructed using two adjacent dominant modes. Comparison of demands estimated using these two interactive relations with those from shake-table tests of two TU building structures (a 1:5-scale five-story reinforced concrete (RC) building model and a 1:12-scale 17-story RC building model) under the service level earthquake (SLE) show that these relations match experimental results of models reasonably well. Concepts proposed in this study enable engineers to not only visualize the overall picture of torsional behavior including the relationship between shear and torsion with the range of forces and deformations, but also pinpoint easily the information about critical responses of structures such as the maximum edge-frame drifts and the corresponding shear force and torsion moment with the eccentricity.

**Keywords:** torsionally-unbalanced; resistance eccentricity; shake-table test; accidental and inherent torsion

## 1. Introduction

Building structures with irregularities are more vulnerable to seismic damage during strong earthquakes. In such buildings, the torsional behavior is one of the most frequent sources of structural damages and failures because the demanded strength and inter-story drift at certain parts of the structure increase due to torsion beyond those required when translational deformation occurs alone. Despite the fact that severe damages or failures of building structures in inelastic torsional responses are of major interest to engineers and researchers, regulations provided by current codes focus only on the elastic behavior.

ASCE 7-10 (2010) specifies two elastic torsion design approaches. One uses an equivalent force (static) procedure, “Where diaphragms are not flexible, the design shall include the inherent torsional moment resulting from eccentricity between the locations of the center of mass (CM) and the center of rigidity (CR) plus the accidental torsional moments caused by assumed displacement of the center of mass each way from its actual location by a distance equal to 5% of the dimension of the structure perpendicular to the direction of the applied forces. Where

earthquake forces are applied concurrently in two orthogonal directions, the required 5% displacement of the center of mass need not be applied in both of the orthogonal directions at the same time but shall be applied in the direction that produces the greater effect.”

The second uses dynamic analysis such as modal response spectrum analysis or time history analysis, where the CM at each story is shifted from its original location in each direction by a distance equal to the accidental eccentricity ( $e_a$ ). The most unfavorable results in terms of member deformations and forces of the structure from dynamic analyses of four positions of the CM in each floor are used for the design.

Although ASCE 7-10 (2010) does not explicitly provide any equation for static design torsion moment, the static design eccentricity,  $e_d$ , is defined with Eqs. (1) and (2) with the situation of static torsion described by Fig. 1(a) (De la Llera and Chopra 1995):

$$e_d = \alpha e_s + \beta b \quad (1)$$

$$e_d = \delta e_s - \beta b \quad (2)$$

where  $e_s$  is the static eccentricity representing the distance between the center of mass (CM) and the center of stiffness or rigidity (CS or CR);  $\beta b$  is the accidental eccentricity ( $e_a$ ) which is included in order to consider torsional effects caused by uncertainties of the CM and the CS, the rotational component of ground motion, and other uncertainties that are not particularly considered;  $b$  is the

\*Corresponding author, Professor Emeritus

E-mail: [hslee@korea.ac.kr](mailto:hslee@korea.ac.kr)

<sup>a</sup>Ph. D. Student

E-mail: [aruth13664@gmail.com](mailto:aruth13664@gmail.com)

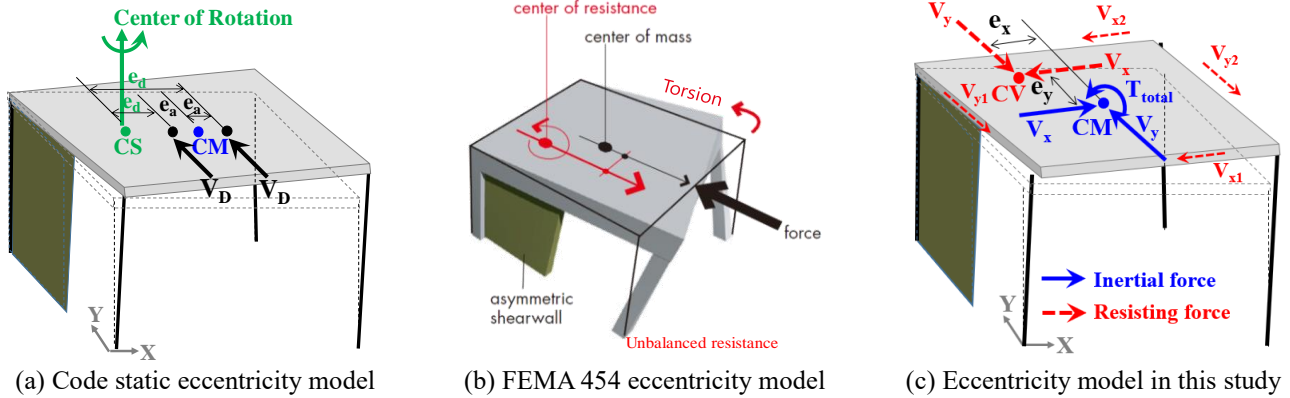


Fig. 1 Eccentricity models

plan dimension of the building perpendicular to the direction of ground motion; and  $\alpha$ ,  $\beta$ , and  $\delta$  are code-specified coefficients whose values vary among building codes:  $\alpha = \delta = 1$  and  $\beta = 0.05$  in the ASCE 7-10 (2010);  $\alpha = 1.5$ ,  $\delta = 1$ , and  $\beta = 0.1$  in the Mexico Federal District Code; and  $\alpha = 1.5$ ,  $\delta = 0.5$ , and  $\beta = 0.1$  in the National Building Code of Canada (De la Llera and Chopra 1995).

Most researchers in the past conducted studies on the elastic behavior of earthquake-induced torsion in building structures based on simplified and idealized models. Some of the publications are discussed below:

De la Llera and Chopra (1994a) have stated the concept and purpose of accidental torsion as “*The accidental torsion is introduced to account for building torsion arising from discrepancies between the mass, stiffness, and strength distributions used in analysis and true distributions at the time of an earthquake; torsional vibrations induced by a rotational motion of the building base; and other sources of torsion not considered explicitly in analysis.*” They have mentioned the impact of accidental torsion on design based on measured records of three nominally symmetric plan building structures: “*Although conceptually appealing, the accidental torsion provision in building codes is a refinement that has a small influence on the sizing and detailing of members and joints for these buildings, especially when considered in the context of many larger approximations inherent in structural design. This investigation supports the experience of many practicing structural engineers that building design is influenced very little by considering the accidental eccentricity of  $\pm 0.05b$ , a code requirement that is cumbersome to implement in design practice.*”

According to Basu *et al.* (2014), “*Accidental torsion is used to indirectly account for: (a) plan distributions of reactive mass that differ from those assumed in design, (b) variations in the mechanical properties of structural components in the seismic force-resisting system, (c) non-uniform yielding of components in the seismic force-resisting system, and (d) torsional ground motion.*”

From this summary, it is somewhat surprising that the use of accidental torsion is extended to indirectly account for the non-uniform yielding of the component in the seismic force-resisting system in controlling inelastic deformations, although the static eccentricity model c

including accidental eccentricity shown in Fig. 1(a) is entirely based on the linear elastic behavior.

De la Llera and Chopra (1994b) have assessed differences between increase in building responses due to accidental eccentricity as estimated by code static and dynamic analyses for symmetric and asymmetric single and multi-story buildings. Their results have indicated that these two approaches predict significantly different increases in design forces resulting from accidental eccentricity. To avoid this discrepancy between design forces measured by code static and dynamic analyses, a new torsion design approach has been proposed by De la Llera and Chopra (1995). This approach can estimate an increase in displacements at the edge of a building resulting from all sources of accidental torsion as a function of the ratio of the plan dimension to the radius of gyration,  $b/r$ , and the fundamental frequency ratio of the uncoupled torsional and lateral motions,  $\Omega$ . The normalized edge displacement,  $u_{b/2}$  (which occur at the distance of the plan dimension,  $b/2$ , from the CM), due to accidental torsion was given as a function of  $\Omega$ . The proposed new procedure has four advantages: (1) it avoids the need for additional structural analyses to account for the effect of accidental torsion; (2) it includes effects of all sources of accidental torsion; (3) it gives a unique value for the increase in a design force due to accidental torsion in the building; and (4) the procedure explicitly states what the expected increase is in design force due to accidental torsion. This approach was later examined by Lin *et al.* (2001) using measured accidental torsion obtained from recorded data of earthquake responses of 12 nominally symmetrical actual buildings. It appeared to be sufficiently accurate for use in design applications accounting for accidental torsion. However, these studies (De la Llera and Chopra 1994b, 1995, Lin *et al.* 2001) mainly focused on the effect of accidental torsion on symmetric-plan building structures with moderate and longer periods.

Lumantarna *et al.* (2018) proposed a Generalized Force Method (GFM), which is essentially a static analysis procedure and is introduced to model the seismically induced displacement demand of low-rise, or medium-rise, buildings featuring uni-axial or bi-axial asymmetry based on the assumption of linear elastic behavior.

Algebraic expressions have been presented to provide

estimates for the edge displacement ratio taking into account the effects of dynamic torsional actions. The expressions have been developed for buildings featuring uni-axial and bi-axial asymmetry. A parametric study conducted by varying torsional stiffness properties and eccentricity values in both directions indicate that buildings with high torsional stiffness are less sensitive to the variations in the value of the eccentricity in both directions. The uni-axial asymmetrical building models is shown to generally result in a conservative prediction of the edge displacement. Also, the maximum displacement of bi-axial asymmetrical building models is shown to be less sensitive to the variations in the value of the eccentricity in the perpendicular direction.

In addition to the above studies on the accidental torsion in the elastic responses of TB building structure, a major portion of research have been devoted to the inelastic behavior of TU structures, and some representative publications among them are introduced below:

Chandler *et al.* (1995) have investigated the influence of accidental eccentricity on the inelastic seismic torsional effect in a building. When calculating the design eccentricity in Eqs. (1) and (2) for the purpose of conducting inelastic dynamic analyses, the eccentricity provision  $\beta = 0.05$  is a reasonable value for torsionally-balanced (TB) systems. However, for torsionally-unbalanced (TU) systems subject to dynamic torsional effects, values of  $\beta > 0.05$  are appropriate. Single-story TU structural models with three y-direction beam-column elements, which provide earthquake resistance and support a rigid floor diaphragm, were adapted in order to investigate effects of new approaches on the ductility and deformation demands. The authors suggested changing values of parameters  $\alpha$ ,  $\delta$ , and  $\beta$  of the design eccentricity by reducing  $\beta$  to a minimum could accordingly increase  $\alpha$  and  $\delta$ . The deformation demands appeared to be satisfactory for systems with moderate torsional stiffness but somewhat over-conservative for systems with low torsional stiffness.

DeBock *et al.* (2014) have quantified the effect of accidental torsion design requirements of codes such as ASCE/SEI 7 on building collapse capacities or collapse risks. To evaluate the building collapse capacity, dynamic analysis was performed for 230 archetypical buildings designed with and without accidental torsion design provisions. The conclusion of their study was *"This study finds that the ASCE/SEI 7 accidental torsion design requirements are only significant (i.e., affecting collapse capacity by 5% or more) for seismic design Category B buildings with torsional irregularity ratio > 1.4 and for seismic design Category D buildings with torsional irregularity ratio > 1.2. When viewed in terms of need, this study found that accidental torsion design requirements are typically not needed (i.e., need < 5%) for any SDC until torsional irregularity ratio > 1.4."*

Stathopoulos and Anagnostopoulos (2010) have investigated the significance and effectiveness of accidental eccentricity using the inelastic model and found that the effectiveness of accidental design eccentricity is limited, opposing the desired effects in the inelastic range. Furthermore, this provision imposes additional

computational requirements on designers and increases structural costs. Hence, they have strongly suggested that the code should abolish accidental design eccentricity provisions for eccentric buildings and only keep them for symmetric buildings. This idea was further reinforced by statements of Anagnostopoulos *et al.* (2015), insisting that the accidental torsion has little effect on member sizing and on making the ductility demand distribution more uniform in the plan; and that *"...more and more people are becoming aware that the vast majority of published work, including most of the papers with code assessment, was based until recently on crude oversimplification and assumption, leaving out essential properties and characteristics of actual buildings. As a consequence, even qualitative conclusions are now questionable and as it has been shown, erroneous trends were often predicted."*

The effect of the transverse frames on the elastic and inelastic seismic demand of TU structures was studied and few researches are introduced as follows:

Lam *et al.* (2016) have suggested a simplified method for assessing seismic drifts of low-rise torsionally-unbalanced building structures in a low-to-moderate seismicity region using acceleration-displacement response spectrum (ADRS) diagrams. In their study, they ignored the contribution of the transverse frame perpendicular to the direction of the excitation to torsional resistance. Hwang *et al.* (2017) have investigated the effect of transverse frames on the seismic drift demand in an extension of the study by Lam *et al.* (2016). Comparing results from these two studies show that there is a significant difference in drift ratio due to the presence or absence of transverse frame perpendicular to the direction of the excitation.

Humar and Kumar (1999) have conducted nonlinear dynamic analysis of a single-story building structure in order to investigate the effect of orthogonal frames in inelastic torsional responses. They also verified the simple static plastic mechanism approach suggested by Paulay first (1998) which could estimate the displacement pattern considering inelastic torsional effects on the seismic response of ductile building structures classified as either "torsionally unrestrained" or "restrained" systems based on the presence or absence of orthogonal frames, respectively. They indicated that displacements obtained by the static plastic mechanism approach for both torsionally unrestrained and torsionally restrained systems differ significantly from those obtained by dynamic analysis since the existence of inertial torsional moment ( $T_{total}$ ) in Fig. 1(c) was ignored in the study by Paulay (1998). Furthermore, results of experimental investigations of a 17-story high-rise torsional unbalance piloti-type RC building (Ko and Lee 2006) and a five-story low-rise torsional unbalanced RC structure (Lee and Hwang 2015) confirmed the existence of large  $T_{total}$  at the CM.

The definition of eccentricity in the code static eccentricity model in Fig. 1(a) differs from the general conception of eccentricity by engineers as given in "designing for earthquake - a Manual for architects" (FEMA 454 2006) (see Fig. 1(b)): *"Torsional forces are created in a building by a lack of balance between the location of the resisting elements and the arrangement of*

the building mass. Engineers refer to this as eccentricity between the center of mass and the center of resistance, which makes a building subjected to ground motion rotate around its center of resistance, creating torsion a twisting action in plan, which results in undesirable and possibly dangerous concentrations of stress.”

According to FEMA 454 (2006), eccentricity is referred to as the resistance eccentricity ( $e_y$ ) defined as the distance between the center of mass and the center of resistance as shown in Fig. 1(b), which is conceptually different from the code static design eccentricity,  $e_d$ , defined as the arm length about the center of rotation as shown in Fig. 1(a).

The code static eccentricity model has two critical shortcomings: (1) the negation of the inertial torsional moment,  $T_{total}$ , at the CM, particularly for TU building structures, and (2) the confusion caused by the discrepancy in the definition of eccentricity  $e_d$  in codes and  $e_y = T_x/V_x$  which is the eccentricity commonly used by engineers such as in FEMA454 (2006). To overcome these shortcomings, a resistance eccentricity model that can accommodate the inertial torsional moment,  $T_{total}$ , at the CM is developed in Fig. 1(c) with advantages of (1) the recognition of the existence of  $T_{total}$  at the CM, (2) the avoidance of the confusion by using  $e_y$  instead of  $e_d$ , and (3) a clear relationship of applied inertial forces at the CM and resisting forces as follows.

$$\begin{aligned} T_{total} &= T_x + T_y = \sum V_{xi} d_{yi} + \sum V_{yi} d_{xi} \\ &= e_y V_x + e_x V_y \end{aligned} \quad (3)$$

$$e_y = T_x / V_x, \quad e_x = T_y / V_y, \quad \eta_y = T_{total} / V_x \quad (4)$$

where  $V_x = \sum V_{xi}$  and  $V_y = \sum V_{yi}$ ;  $i$  represents frame numbers in X and Y directions, respectively;  $T_{total}$  is the sum of torsional moments resisted to by X-directional ( $T_x$ ) and Y-directional ( $T_y$ ) frames; and  $d_{xi}$  and  $d_{yi}$  are distances of the  $i$ -th frame in X and Y directions, respectively, from the CM (see Fig. 1(c)). In the resistance eccentricity model outlined in Fig. 1(c), general relationships of forces in a single-story building under earthquake can be described with inertial forces ( $V_x$ ,  $V_y$ ,  $T_{total}$ ) at the CM and resisting resultant shear forces located at eccentricities  $e_x$ ,  $e_y$  and  $\eta_y$  as shown in Eqs. (3) and (4).

Very few studies have examined the adequacy of the basic concept (or assumption) of the current code static torsional design approach in the elastic response, particularly for TU buildings. The direct relationship between elastic shear and torsion is also yet to be investigated in detail. In this study, using the resistance eccentricity model as described above (Fig. 1(c)), the following two interactive relations between shear and torsion are proposed: (1) seismic responses of a structure such as  $\delta_{edge}/\delta_{center}$ ,  $\mu_x = \theta_t/\delta_{center}$ ,  $\eta_y = T_{total}/V_x$ , and  $T_x/T_{total}$  at instants of peak edge-frame drifts are given as functions of  $e_y = T_x/V_x$ , and (2) hysteretic relationships between shear and torsion in forces and deformations are bounded by ellipsoids constructed by using two adjacent dominant modes. Demands estimated using these two interactive relations are compared with those from shake-table tests of

two TU building structures (a 1:5-scale five-story reinforced concrete (RC) building model and a 1:12-scale 17-story RC building model) under the service level earthquake (SLE). The significance of these findings is then discussed in detail with respect to the code static torsion design.

## 2. Basic concepts for prediction of seismic elastic torsional demand

### 2.1 Prediction of critical torsional behaviors as functions of resistance eccentricity

For a general single-story two-way asymmetric structural system, the story force vector  $\{V_x, V_y, T_{total}\}$  at the CM is related to the inter-story drift vector  $\{\delta_x, \delta_y, \theta_t\}$  at the CM as shown in Eq. (5) at instants of peak edge-frame drifts when the velocity becomes zero and, therefore, the resisting force by frames becomes equal to the inertia force in the dynamic equilibrium equation. Using Eq. (5), ratios of the peak edge-frame drifts to the central drift ( $\delta_{edge}/\delta_{center}$ ), the total torsional moment to the shear force ( $\eta_y = T_{total}/V_x$ ), and the torsional moment resisted by X-directional frames to the total torsional moment ( $T_x/T_{total}$ ) are derived as functions of the resistance eccentricity,  $e_y = T_x/V_x$  in Eqs. (7) - (12) (For details, refer to Appendix A). Even when the structure has a bi-directional asymmetric plan,  $\gamma_y = V_x/V_y$  affects only  $e_y = T_x/V_x$ ,  $\eta_y = T_{total}/V_x$  and  $T_x/T_{total}$  as shown in Eqs. (8) - (10).

$$\begin{Bmatrix} V_x \\ V_y \\ T_{total} \end{Bmatrix} = \begin{bmatrix} K_X & 0 & K_{\theta X} \\ 0 & K_Y & K_{\theta Y} \\ K_{\theta X} & K_{\theta Y} & K_{\theta\theta} \end{bmatrix} \begin{Bmatrix} \delta_x \\ \delta_y \\ \theta_t \end{Bmatrix} \quad (5)$$

$$\delta_x = \frac{V_x - \theta_t K_{\theta X}}{K_X} \quad (6a)$$

$$\delta_y = \frac{V_y - \theta_t K_{\theta Y}}{K_Y} \quad (6b)$$

$$\theta_t = \frac{T_{total} - e_y V_x - e_x V_y}{K_{\theta s}} \quad (6c)$$

where  $K_X$  and  $K_Y$  are the story lateral stiffness in X and Y directions, respectively;  $K_{\theta X} = e_{sy} K_X$  and  $K_{\theta Y} = e_{sx} K_Y$  are the coupled lateral and torsional stiffness in X and Y directions, respectively;  $K_{\theta\theta}$  is the torsional stiffness about the CM, which is the sum of  $K_{\theta\theta X}$  and  $K_{\theta\theta Y}$ , the contributions by X and Y directional frames, respectively;  $K_{\theta s} = (K_{\theta\theta X} - e_{sy}^2 K_X) + (K_{\theta\theta Y} - e_{sx}^2 K_Y)$  is the torsional stiffness about the CS, which is the sum of  $K_{\theta s X}$  and  $K_{\theta s Y}$ , the contributions by X and Y directional frames, respectively.

$$e_y = \frac{T_x}{V_x} = \frac{\delta_x K_{\theta X} + \theta_t K_{\theta\theta X}}{\delta_x K_X + \theta_t K_{\theta X}} \quad (7)$$

Substituting Eqs. (6a) and (6c) and using  $\eta_y = T_{total}/V_x$  to

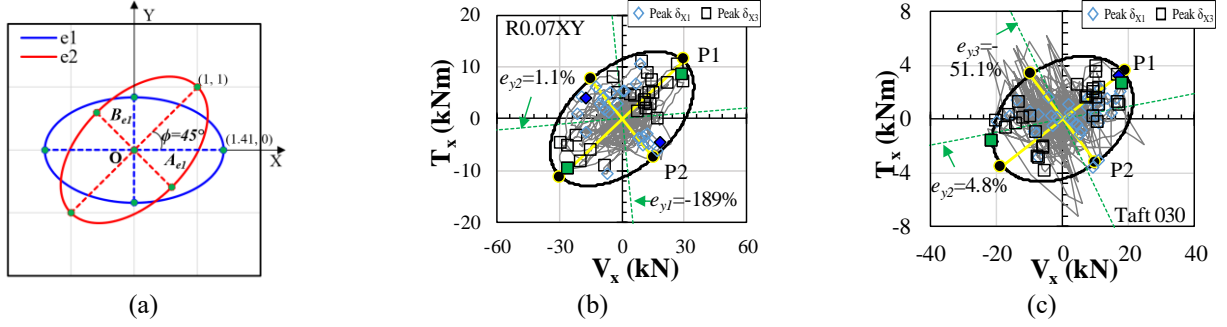


Fig. 2 (a) Typical ellipse with  $\phi=0$  and  $45^\circ$ , (b) relationships between  $T_x$ - $V_x$  for five-story model and (c) relationships between  $T_x$ - $V_x$  for 17-story model

Table 1 Values of P1, P2,  $A_{el}$  and  $B_{el}$  for five-story and 17-story models

		Five-story model	17-story model
$V_x$ (kN)	P1	29.9	18.8
	P2	15	9.85
$T_x$ (kNm)	P1	11.3	3.57
	P2	-7.59	-3.29
$A_{el}$		1.41	1.41
$B_{el}$		0.83	1.06

Eq. (7), the following equations are obtained:

$$e_y = \left( \frac{K_{\theta\theta X} - e_{sy}^2 K_X}{K_{\theta\theta} - e_{sy}^2 K_X - e_{sx}^2 K_Y} \right) (\eta_y - e_{sx} \gamma_y) + \left( \frac{K_{\theta\theta Y} - e_{sx}^2 K_Y}{K_{\theta\theta} - e_{sy}^2 K_X - e_{sx}^2 K_Y} \right) e_{sy} \quad (8)$$

$$= b_x (\eta_y - e_{sx} \gamma_y) + b_y e_{sy}$$

where

$$\gamma_y = V_x / V_y,$$

$$b_x = \frac{K_{\theta SX}}{K_{\theta S}} = \frac{K_{\theta\theta X} - e_{sy}^2 K_X}{K_{\theta\theta} - e_{sy}^2 K_X - e_{sx}^2 K_Y},$$

$$b_y = \frac{K_{\theta\theta Y} - e_{sx}^2 K_Y}{K_{\theta\theta} - e_{sy}^2 K_X - e_{sx}^2 K_Y}, \text{ and}$$

$$\eta_y = T_{total} / V_x = \left( (e_y - b_y e_{sy}) / b_x \right) + e_{sy} \gamma_y. \quad (9)$$

And,

$$\frac{T_x}{T_{total}} = \frac{1}{T_{total} / V_x} e_y = \frac{1}{\eta_y} e_y = \frac{e_y b_x}{e_y - (b_y e_{sy} - b_x e_{sy} \gamma_y)} \quad (10)$$

$$\mu_x = \frac{\theta_t}{\delta_x} = \frac{e_y - e_{sy}}{(K_{\theta\theta} / K)_X - e_{sy} e_y} \quad (11)$$

$$\frac{\delta_{stiff}}{\delta_x} = 1 + \mu_x d_{y,stiff} \quad \text{or} \quad \frac{\delta_{flex}}{\delta_x} = 1 + \mu_x d_{y,flex} \quad (12)$$

where  $\delta_{stiff}$  and  $\delta_{flex}$  are story drifts at the stiff edge and the flexible edge, respectively; and  $d_{y,stiff}$  and  $d_{y,flex}$  are distances of the stiff edge and flexible edge, respectively, from the CM. The reliability of Eqs. (7) - (12) is evaluated by

comparing with experimental data.

## 2.2 Bounding of seismic demands with ellipses

Lee and Hwang (2015) have suggested that instead of using a specific value of eccentricity as a design parameter, the demand in torsion can be determined in the direct relationship with the base or story shear represented as an ellipse constructed with the maximum points in its principal axes located by two adjacent dominant modal spectral values. In this study, hysteretic relationships between shear and torsion in forces and deformations are bounded by the ellipsoids constructed using two adjacent dominant modes.

This approach can provide a simple but transparent conceptual design tool.

The elliptical boundaries given in Figs. 2(b) and 2(c) are derived in 4 steps: (1) normalize the coordinates of the maximum points P1( $V_{x1}$ ,  $T_{x1}$ ) and P2( $V_{x2}$ ,  $T_{x2}$ ) of ellipsoid by ( $V_{x1}/V_{x1}$ ,  $T_{x1}/T_{x1}$ ) and ( $V_{x2}/V_{x1}$ ,  $T_{x2}/T_{x1}$ ), respectively; (2) construct the ellipse  $e1$  (with  $\phi=0$ ) with

$$A_{e1} = \sqrt{(V_{x1}/V_{x1})^2 + (T_{x1}/T_{x1})^2} = \sqrt{2} \quad \text{and} \quad B_{e1} = \sqrt{(V_{x2}/V_{x1})^2 + (T_{x2}/T_{x1})^2} \quad \text{in}$$

Fig. 2(a); and the coordinates  $X_{e1}(t)$  and  $Y_{e1}(t)$  of ellipse  $e1$  for the range of  $t$ ,  $0 \leq t \leq 2\pi$ , will be  $A_{e1} \cos(t)$  and  $B_{e1} \sin(t)$ , respectively, shown as the blue ellipsoid in Fig. 2(a); (3) the coordinates of ellipse  $e2$ ,  $X_{e2}(t)$  and  $Y_{e2}(t)$ , are determined by Eq. (13) for an angle of  $\phi=45^\circ$  (or  $135^\circ$  if  $V_{x1}$  is negative) shown as the red ellipsoid in Fig. 2(a); and finally (4) the elliptical boundary for the hysteretic relation of  $T_x$ - $V_x$  will be obtained by multiplying  $X_{e2}(t)$  by the  $V_{x1}$  and  $Y_{e2}(t)$  by  $T_{x1}$ . Elliptical boundaries for the five-story model and the 17-story model are constructed by using the information in Table 1. The determination of points P1 and P2 in Table 1 will be explained in detail later in this paper.

Rotation coords

$$\begin{Bmatrix} X_{e2}(t) \\ Y_{e2}(t) \end{Bmatrix} = \begin{bmatrix} \cos(\phi) & -\sin(\phi) \\ \sin(\phi) & \cos(\phi) \end{bmatrix} \times \begin{Bmatrix} A_{e1} \times \cos(t) \\ B_{e1} \times \sin(t) \end{Bmatrix} \quad (13)$$

Rotated coordinates

$$= \begin{bmatrix} A_{e1} \times \cos(t) \times \cos(\phi) - B_{e1} \times \sin(t) \times \sin(\phi) \\ A_{e1} \times \cos(t) \times \sin(\phi) + B_{e1} \times \sin(t) \times \cos(\phi) \end{bmatrix}$$

where  $t$  is the parametric angle which will go to full circle,  $0 \leq t \leq 2\pi$ ;  $A_{e1}$  is the radius in the major axis;  $B_{e1}$  is

Table 2 Assessment of irregularities according to KBC 2005 (AIK 2005) and KBC 2000 (AIK 2000) for the five-story and 17-story prototype

Irregularity	Criteria*	Five-story				17-story prototype
		Original prototype		Strengthened prototype		
		X-dir.	Y-dir.	X-dir.	Y-dir.	X-dir.
Stiffness	If $K_i/K_{i+1} < 0.7$ , irregular	0.159	0.160	0.218	0.213	0.430
Strength	If $F_i/F_{i+1} < 0.8$ , irregular	0.181	0.284	0.260	0.326	0.40
Torsion	If $\delta_{max}/\delta_{avg} > 1.2$ , irregular	1.18	1.82	1.26	1.31	1.72

\* where  $K_i/K_{i+1}$ : stiffness of  $i^{th}$  story/ stiffness of  $(i+1)^{th}$  story;  $F_i/F_{i+1}$ : strength of  $i^{th}$  story/ strength of  $(i+1)^{th}$  story; and  $\delta_{max}/\delta_{avg}$ : maximum edge-frame drift / average drift at one story.



(a) Original model



(b) Strengthened model

Fig. 3 Overview of earthquake simulation test set-up for the five-story model: (a) Original model and (b) Strengthened model (Lee *et al.* 2011, 2013)

the radius in the minor axis; and  $\phi$  is the angle between the X-axis and the major axis of the ellipse.

### 3. Description of experimental RC TU building structure models

#### 3.1 Five-story RC building structure model

A prototype building was determined based on inventory data on low-rise piloti-type RC residential buildings in Korea (Lee *et al.* 2011). Reinforcement details are non-seismic according to typical construction practices in Korea. The prototype has extreme irregularities of a soft/weak story and torsion at the ground story. To reduce these irregularities, the model was strengthened by implementing buckling-restrained braces (BRBs) and fiber-reinforced polymer (FRP) sheets in peripheral frames at the ground story, thereby satisfying the seismic design code, Korean Building Code (KBC) 2005 (AIK 2005). The lowest two stories of the 1:5-scale test specimens were designed and constructed in order to strictly satisfy the similitude-law

requirements, while the upper three stories were replaced with concrete blocks of similar volumes as shown in Fig. 3. This modified model reduced both the time and cost needed for the construction without causing a significant loss of similitude in the response. The seismic weight,  $W$ , of the 1:5-scaled strengthened specimen is 267.4 kN and the design base shear is  $V_d = 47.1$  kN. Detailed information on the design of the strengthened model is provided in the study of Lee *et al.* (2013). Values of torsional irregularity in accordance with KBC 2005 (AIK 2005) and ASCE 7-10 (2010) for the original prototype are given as 1.18 and 1.82 in the X-direction and the Y-direction, respectively. For the strengthened prototype, these values are given as 1.26 and 1.31 in the X-direction and the Y-direction, respectively. Results of assessment of irregularity at the ground floor for the five-story prototype according to KBC 2005 (AIK 2005) are summarized in Table 2. The range of the design eccentricity of the strengthened prototype in the X direction is  $e_d = 16.3\% \pm 1.1 \times 5\% = 10.8\%$  to 21.8% of the plan width as calculated from the design stiffness.

Initial stiffness values of strengthened frames X3, Y1, and Y4 as obtained from shake-table tests were significantly lower than design values, being rather close to those of original frames (Lee *et al.* 2013, Lee and Hwang 2015). The strengthened experimental model revealed torsionally-flexible two-way asymmetric behaviors with  $e_{sy} = 1.33\%$  and  $e_{sx} = -2.9\%$ .

The first series of earthquake simulation tests of the original model were conducted up to the level of the design earthquake (DE) in Korea in 2009, at the Korea Institute of Machinery and Materials as shown in Fig. 3(a) (Lee *et al.* 2011). The second series of earthquake simulation tests of the strengthened model were carried out at the Seismic Simulation Test Center at Pusan National University, Korea in 2010 (Fig. 3(b)) (Lee *et al.* 2013, Lee and Hwang 2015). The experimental set-up and instrumentation to measure displacements, accelerations, and forces of strengthened model are shown in Fig. 4.

The target or input accelerogram of the table was based on the recorded 1952 Taft N21E (X direction) and Taft S69E (Y direction) components. It was formulated by compressing the time axis with a scale factor of  $1/\sqrt{5}$  and adjusting the peak ground acceleration (PGA) to match the corresponding elastic design spectrum in KBC 2005 (AIK 2005). A service level earthquake (SLE) is defined as the level of  $PGA = 0.07$  g with 1952 Taft N21E and S69E



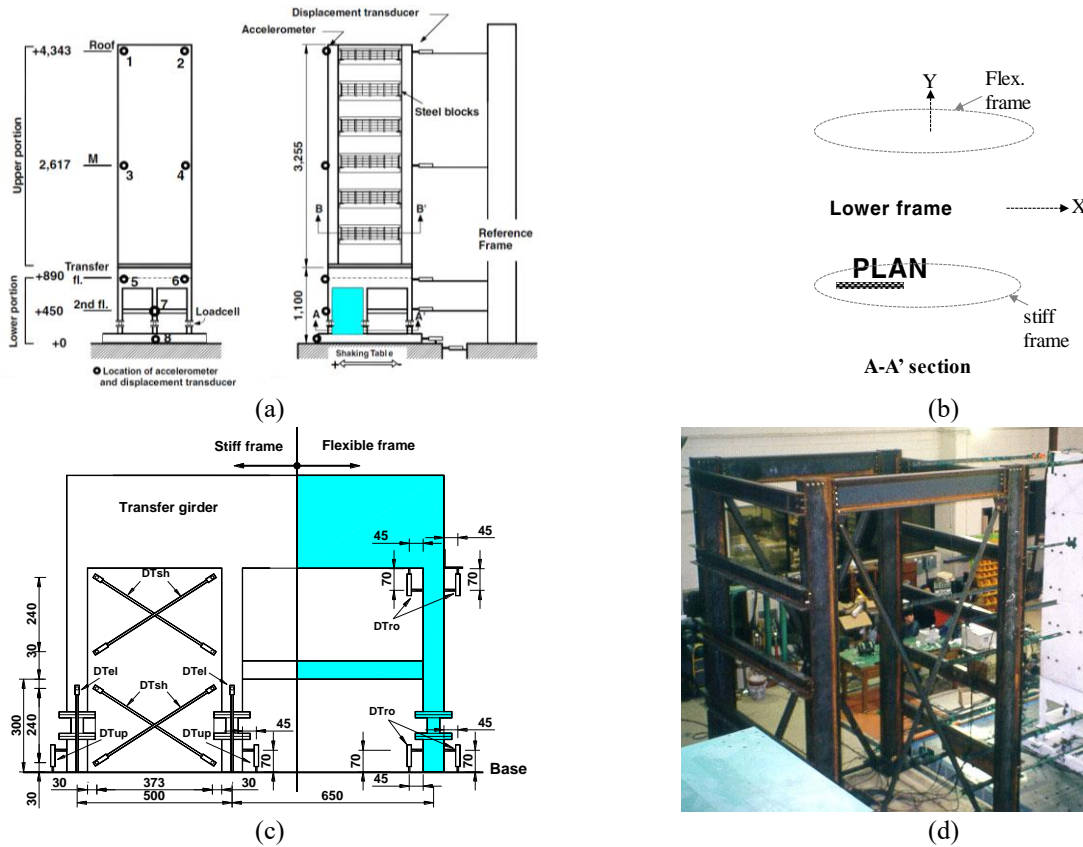


Fig. 6 Experimental arrangement (unit: mm) for the 17-story model. (a) Front view and side view; (b) Plan; (c) Instrumentation for wall and columns and (d) Overview of the experimental arrangement (Ko and Lee 2006)

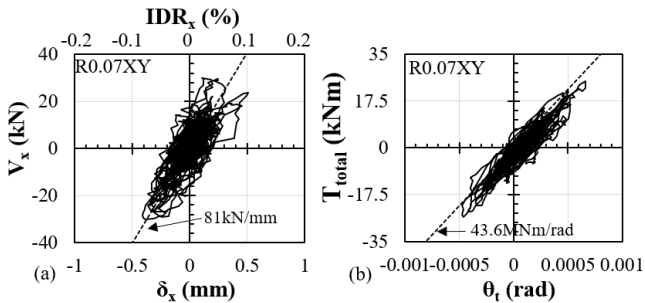


Fig. 7 Hysteretic relations between (a)  $V_x-\delta_x$  and (b)  $T_{total}-\theta_t$  for the five-story model

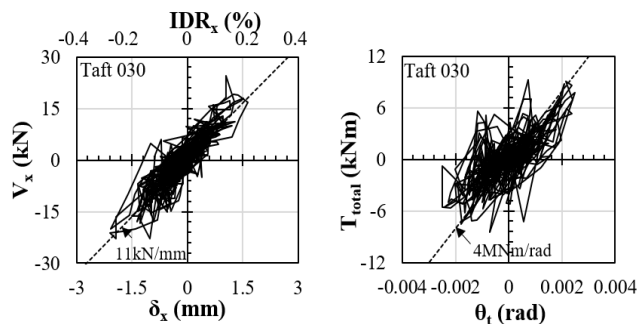


Fig. 8 Hysteretic relations between (a)  $V_x-\delta_x$  and (b)  $T_{total}-\theta_t$  for the 17-story model

Custom-made load cells were installed at mid-heights of all columns in the first story to measure shear forces. The

elevation and plan of the model as well as the experimental set-up and the instrumentation used to measure displacements, accelerations, and forces are shown schematically in Figs. 6(a), 6(b) and 6(c). The reference frame for measuring the lateral displacement of the model was established outside the shaking table as shown in Fig. 6(d).

#### 4. Experimental performances of the two structure models

Hysteretic responses from experimental results of the five-story model and the 17-story model are presented in Figs. 7 and 8, respectively. As shown in Fig. 7(a), shear hysteretic curves of  $V_x-\delta_x$  exhibit an elastic response with lateral stiffness  $K_x = 81 \text{ kN/mm}$ . The torsional hysteretic curve of  $T_{total}-\theta_t$  in Fig. 7(b) also shows an elastic response with  $K_{\theta\theta} = 43.6 \text{ MNm/rad}$ . The ratio of the maximum base shear force to the weight of the model ( $= 29.8 \text{ kN}/247.4 \text{ kN} = 0.12$ ) is 12% under the SLE. In Fig. 8(a), shear hysteretic curves of  $V_x-\delta_x$  exhibit an elastic response with lateral stiffness  $K_x = 11 \text{ kN/mm}$ . The torsional hysteretic curve of  $T_{total}-\theta_t$  in Fig. 8(b) also shows an elastic response with  $K_{\theta\theta} = 4 \text{ MNm/rad}$ . The ratio of the maximum base shear force to the weight of the model ( $= 24.5 \text{ kN}/(92 \times 2 \text{ kN}) = 0.135$ ) is 13.5%, corresponding to the DE with a return period of 500 years in the old Korean seismic code KBC 2000 (AIK 2000).

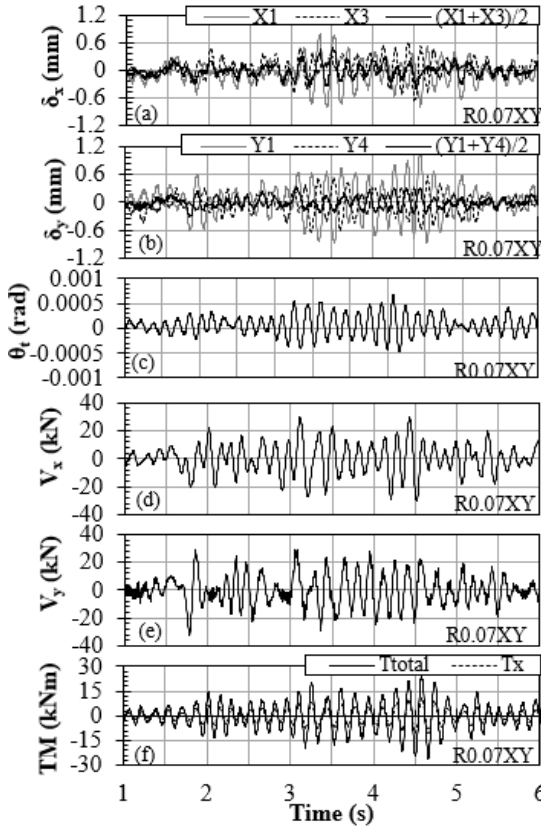


Fig. 9 Time histories of (a)  $\delta_{x1}$ ,  $\delta_{x3}$ ,  $\delta_x$ ; (b)  $\delta_{y1}$ ,  $\delta_{y4}$ ,  $\delta_y$ ; (c)  $\theta_t$ ; (d)  $V_x$ ; (e)  $V_y$ ; and (f)  $T_{total}$  and  $T_x$  for the five-story model

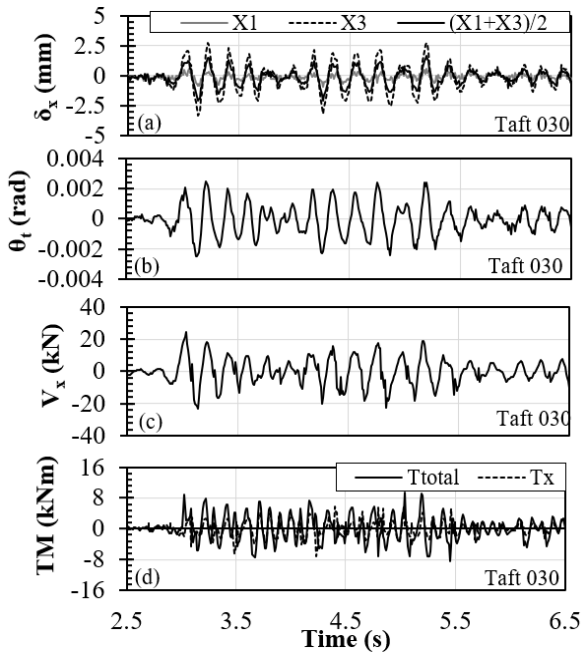


Fig. 10 Time histories of (a)  $\delta_{x1}$ ,  $\delta_{x3}$ ,  $\delta_x$ ; (b)  $\theta_t$ ; (c)  $V_x$ ; and (d)  $T_{total}$  and  $T_x$  for the 17-story model

For the five-story model, Figs. 9(a), 9(b) and 9(c) show time histories of inter-story drifts,  $\delta_x = (\delta_{x1} + \delta_{x3})/2$ ,  $\delta_{x1}$ , and  $\delta_{x3}$  in the X-direction,  $\delta_y = (\delta_{y1} + \delta_{y4})/2$ ,  $\delta_{y1}$ , and  $\delta_{y4}$  in the Y-direction, and the torsional deformation,  $\theta_t$ , of the model at the ground story. Figs. 9(d), 9(e) and 9(f) show time

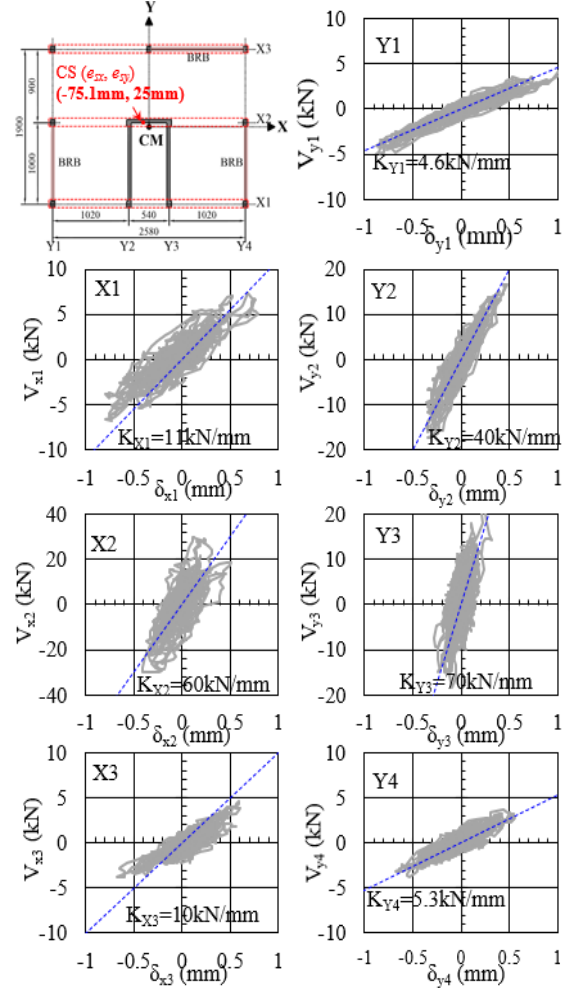


Fig. 11 Shear hysteretic curves ( $V$ - $\delta$ ) of all the frames of the five-story model

histories of base shears,  $V_x$  and  $V_y$ , and base torsional moments,  $T_{total}$  and  $T_x$ . For the 17-story model, Figs. 10(a) and 10(b) show time histories of inter-story drifts,  $\delta_x$ ,  $\delta_{x1}$ , and  $\delta_{x3}$  in the X-direction and the torsional deformation,  $\theta_t$ , of the model at lower two stories beneath the transfer floor in Fig. 6(a). Figs. 10(c) and 10(d) show time histories of base shear,  $V_x$ , and base torsional moments,  $T_{total}$  and  $T_x$ .

## 5. Verification of proposed concepts through comparison with test results

### 5.1 Global responses

For the five-story model, shear forces in each frame were obtained from load cells in both X and Y directions. For the 17-story model, only shear forces in Frame X2 and Frame X3 were obtained from load cells while the shear force in Frame X1 was calculated by subtracting shear forces in X2 and X3 from the total inertial force in the X direction. As properties of columns in Frames X2 and X3 are the same as those of all columns in frames in the Y-direction, the stiffness in each frame is assumed to be equal to that in Frames X2 and X3 ( $K_{X2} = K_{X3} = K_{Y1} = K_{Y2} = K_{Y3}$ ).

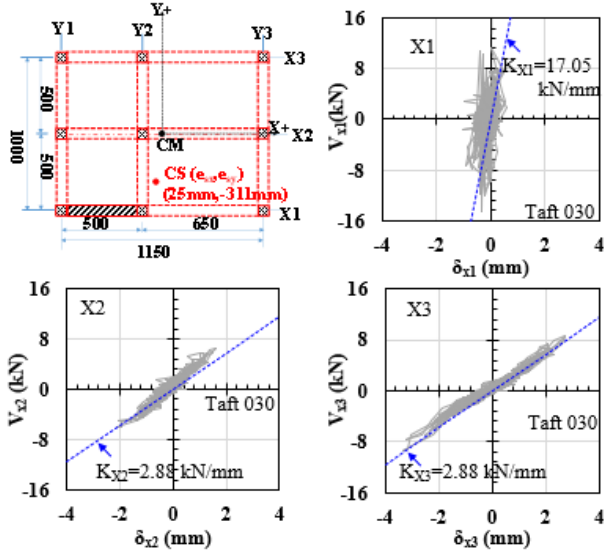


Fig. 12 Shear hysteretic curves ( $V$ - $\delta$ ) of frames X1, X2 and X3 of the 17-story model

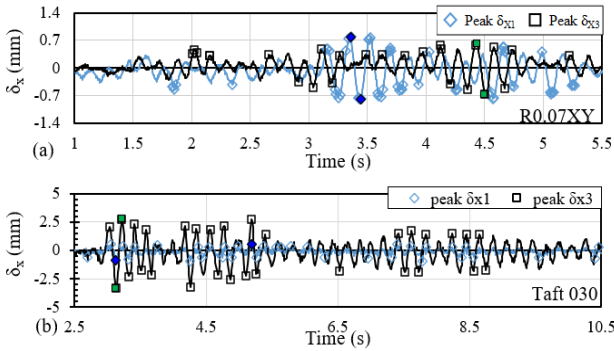


Fig. 13 Time history of edge-frame drifts ( $\delta_{x1}$  and  $\delta_{x3}$ ) for (a) the five-story and (b) the 17-story models

Values of elastic stiffness presented in Table 3 are estimated from shear hysteretic curves ( $V$ - $\delta$ ) of each frame of the five-story and the 17-story models shown in Figs. 11 and 12, respectively.

In the time history of displacement shown in Fig. 13, the data points represent the peak edge-frame drifts in Frames X1 (blue diamond markers) and X3 (black square markers) at the ground story for both models, which correspond to time instants of zero velocity; that is, the state when the resisting force by the frames is equal to the inertia force. They are selected only if the peak edge-frame drifts exceed one-half of the maximum positive and negative drifts for the five-story and 17-story models. The maximum peak points are denoted as blue solid diamond for  $\delta_{x1}$  and green solid rectangle for  $\delta_{x3}$ . Elastic time history analyses were performed using an equivalent single-story three-degree-of-freedom system with the stiffness given in Table 3. Modal periods for both models obtained by applying Fast Fourier transform (FFT) to experimental data and modal analyses for equivalent single-story models are given in Table 4.

For the five-story model, the first mode is a torsional mode whereas the second is a X-directional translational mode as shown in Fig. 14(a). However, for the 17-story

Table 3 Values of elastic stiffness in Eq. (5) for five- and 17-story models

	Models	
	Five-story	17-story
$K_X$ (kN)	81	22.8
$K_Y$ (kN)	120	8.64
$K_{\theta X} = e_{sy}K_X$ (kN/rad)	2050	-7085
	( $e_{sy}=25.3=1.33\%$ )	( $e_{sy}=-311=-31.1\%$ )
$K_{\theta Y} = e_{sx}K_Y$ (kN/rad)	-9003	216
	( $e_{sx}=-75.1=-2.9\%$ )	( $e_{sx}=25.0=2.17\%$ )
$K_{\theta\theta X}$ (kNmm/rad)	$19.1 \times 10^6$	$4.98 \times 10^6$
$K_{\theta\theta Y}$ (kNmm/rad)	$24.5 \times 10^6$	$1.92 \times 10^6$
$K_{\theta\theta}$ (kNmm/rad)	$43.6 \times 10^6$	$6.90 \times 10^6$

Table 4 Periods of five- and 17-story models

		Period in sec	
		Experiment	Modal analysis
Five-story model	Mode 1	0.18	0.182
	Mode 2	0.171	0.138
	Mode 3	0.161	0.113
17-story model	Mode 1	0.203	0.225
	Mode 2	0.195	0.191
	Mode 3	0.092	0.106

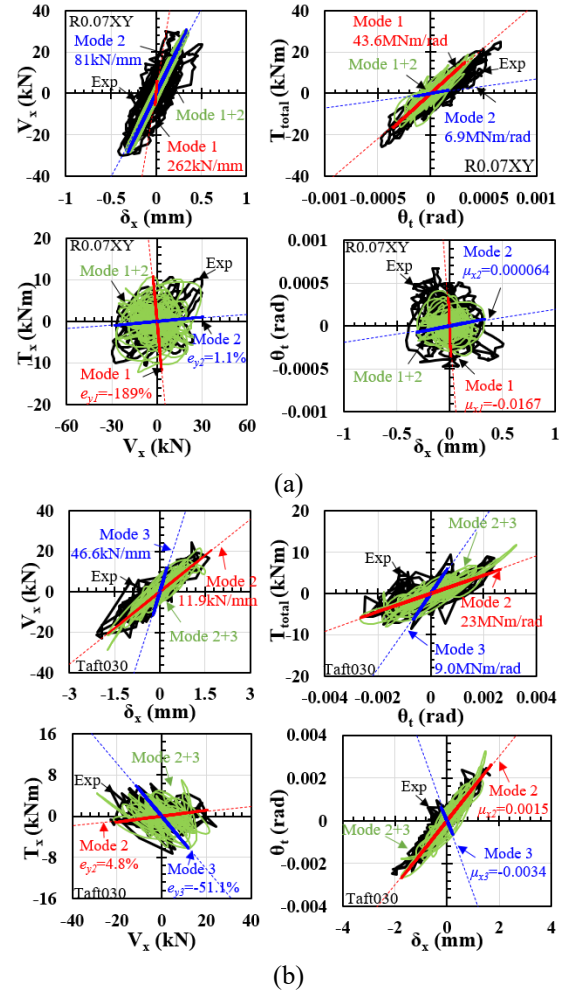


Fig. 14 Analytical results compared with experimental response histories of  $V_x$ - $\delta_x$ ,  $T_{total}$ - $\theta_t$ ,  $T_x$ - $V_x$ , and  $\theta_t$ - $\delta_x$  for (a) the five-story model and (b) the 17-story model

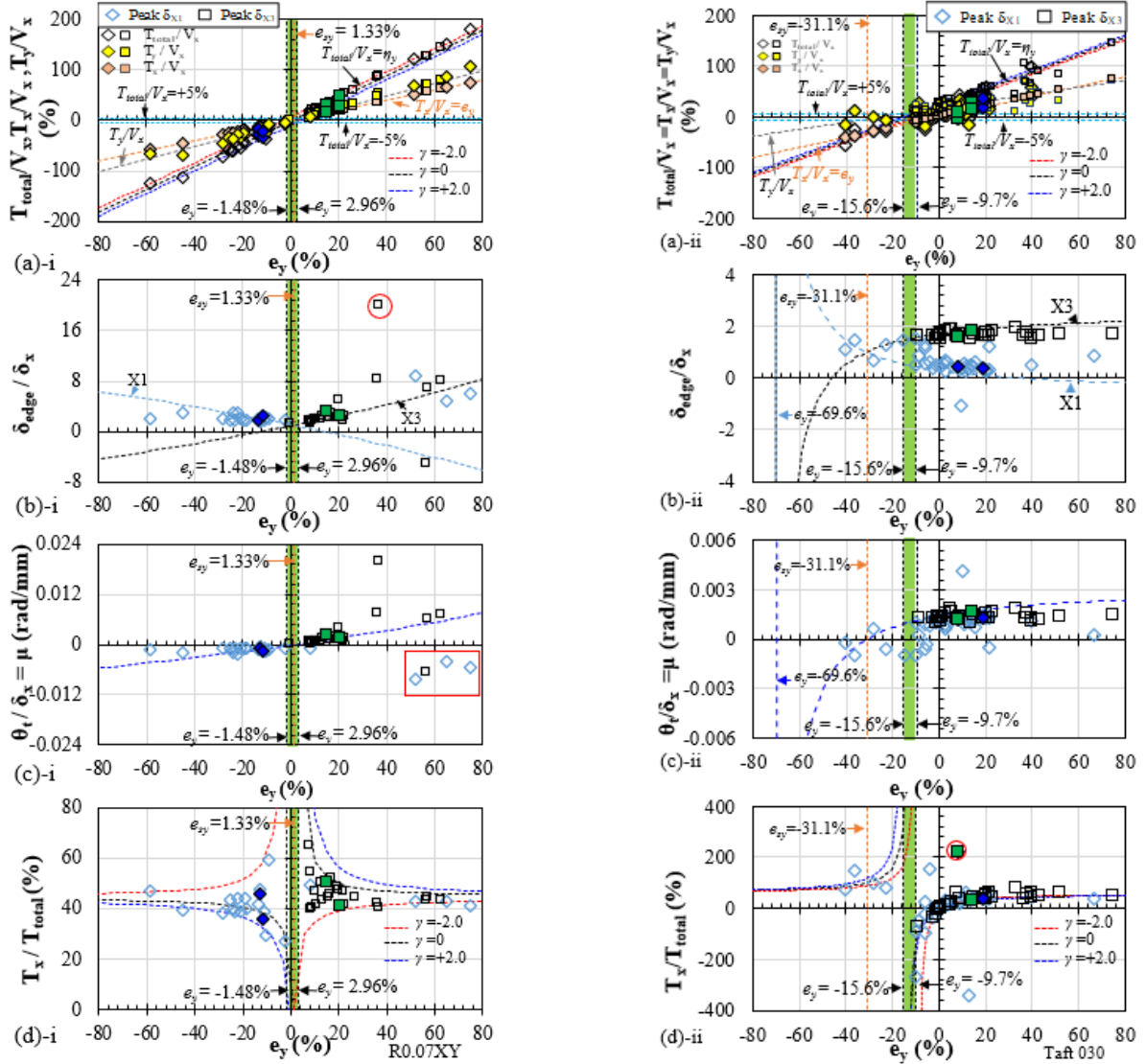


Fig. 15 Distributions of critical responses of (a)  $T_{total}/V_x$ ;  $T_x/V_x$ ;  $T_y/V_x$ ; (b)  $\delta_{edge}/\delta_x$ ; (c)  $\theta_t/\delta_x$ ; and (d)  $T_x/T_{total}$  at instants of peak  $\delta_{edge}$  compared to prediction equations for: i) the five-story and ii) the 17-story models

model, the first mode is a translational mode in the Y direction which is not of interest and the second mode is the predominant mode coupled by the translation in the X-direction and minor torsion while the third mode is the major mode governing torsion that can be noticed in Fig. 14(b). For the five-story model, the shear stiffness of the second mode with the torsional stiffness of the first mode represents the overall shear and torsional stiffnesses in experiment as shown in Fig. 14(a). However, for the 17-story model, the second mode represents both the shear stiffness and the torsional stiffness in the experiment as shown in Fig. 14(b), although the influence of the third mode is not negligible in the hysteretic curve of  $T_x-V_x$ . It is interesting to note that the combination of only two adjacent governing modes for five-story and 17-story models simulates experimental behaviors very well in Fig. 14. For the five-story model, modal eccentricities ( $e_{y,i} = T_{x,i}/V_{x,i}$  for the  $i$ -th mode) are  $e_{y,1} = -189\%$  and  $e_{y,2} = 1.1\%$  for the first mode and the second mode, respectively. For the 17-story model, modal eccentricities are  $e_{y,2} = 4.8\%$  and  $e_{y,3} = -51.1\%$

for the second mode and the third mode, respectively.

## 5.2 Comparison of experimental responses at peak edge-frame drifts with prediction equations

In Eq. (9), the ratio  $\eta_y = T_{total}/V_x$  is given as a linear function of  $e_y = T_x/V_x$  with the term of  $\gamma = V_x/V_y$ . For the five-story model, the black, blue and red dashed lines are plotted in Fig. 15 (a)-i for  $\gamma = 0, +2$ , and  $-2$ , respectively. The range of  $T_{total}/V_x$  within boundaries corresponding to  $\gamma = \pm 2$  cover experimental data. Also, it is found that  $\gamma$  has a negligible effect on the overall linearity of  $T_{total}/V_x$  with respect to  $e_y$ . For the 17-story model, more scatters could be seen. However, the general trend of experimental data coincides with the dashed lines of Eq. (9) in Fig. 15 (a)-ii. Distributions of responses at instants of peak edge-frame drifts are compared with prediction Eqs. (8) - (12) for the five-story model and the 17-story model in Figs. 15(b)-(d). Ratios of  $\delta_{stiff}/\delta_x$ ,  $\delta_{flex}/\delta_x$ , and  $\mu_x = \theta_t/\delta_x$  asymptotically approach to  $1-d_{y/stiff}/e_{sy}$ ,  $1-d_{y/flex}/e_{sy}$ , and  $-1/e_{sy}$ , respectively,

Table 5 Experimental values of responses at the maximum or minimum edge-frame drifts

	Models		
	Five-story		17-story
$\delta_{edge}$	$\delta_{x1,min}$	$\delta_{x3,min}$	both ( $\delta_{x1,min}$ and $\delta_{x3,min}$ )
$e_y$ (%)	-11.6	20.5	8.06
$\eta_y$ (%)	-32.4	49.5	3.64
$\delta_{x1}$ (mm)	-0.79	0.125	-0.86
$\delta_{x3}$ (mm)	0.127	-0.67	-3.34
$\delta_x$ (mm)	-0.33	-0.27	-2.1
$V_x$ (kN)	-17.6	-25.5	-21.3
$T_x$ (kNm)	3.89	-9.9	-1.72
$T_{total}$ (kNm)	10.9	-23.9	-0.78
$\theta_t$ ( $\times 10^{-4}$ rad)	4.9	-4.2	-24.9
$\delta_{edge}/\delta_x$	2.4	2.5	1.59

when  $e_y$  goes to the negative infinity for the five-story model and when  $e_y$  goes to the positive infinity for the 17-story model in Fig. 15(b).

These ratios,  $\delta_{stiff}/\delta_x$  and  $\delta_{flex}/\delta_x$ , become infinite when rotation with no translation become predominant movement at  $e_y = -69.6\%$  for the 17-story model in Figs. 15 (b)-ii and (c)-ii shown as a vertical line, but not visible for the five-story model due to the given range of  $e_y$  in Figs. 15 (b)-i and (c)-i being exceeded by  $e_y = 490\%$ , the eccentricity representing the torsional movement only.

The data point corresponding to the ratio of  $\delta_{x3}/\delta_x = 20.0$  (0.327 mm/0.016 mm) at  $e_y = +36.6\%$  (the data point inside the red circle in Fig. 15 (b)-i) is far from the prediction ( $\delta_{x3}/\delta_x = 3.90$ ). This is because, at the instant, the drift at the center,  $\delta_x$ , is so small and values of drifts at Frames X1 and X3 are almost similar but opposite in the direction ( $\delta_{flex} = -0.29$  mm and  $\delta_{stiff} = 0.33$  mm). Also, in Fig. 15 (c) - (i), experimental data points of  $\theta_t/\delta_x$  inside the red rectangle appear to be far from the prediction for the similar reason.

Experimental data of forces and drifts at instants of the maximum and minimum peak edge-frame drifts in Table 5 are denoted as blue solid diamond ( $\delta_{x1}$ ) and green solid rectangle ( $\delta_{x3}$ ) markers in Figs. 13 and 15 for the five-story model and the 17-story model. For the five-story model, in Table 5, the value of  $\delta_{x3}$  is relatively smaller in the opposite direction when  $\delta_{x1}$  attains its maximum and vice versa. For the 17-story model both maximum  $\delta_{x1}$  and  $\delta_{x3}$  occur at the same instant, with a very small  $T_{total}$  (see also the red circle in Fig. 18 (d)-ii), leading to a large ratio of  $T_x/T_{total}$  (see the red circle in Fig. 15 (d)-ii). Maximum drifts ratios,  $\delta_{edge}/\delta_x$ , for the five-story model are 2.4 and 2.5 in the Table 5. They are much larger than the values of drift ratios obtained by using the 5% accidental torsion in Table 2, 1.26. But for the 17-story model, the maximum drift ratio 1.59 in Table 5 appears to be comparable to 1.72 in Table 2.

Fig. 15 (d) shows that  $T_x/T_{total}$  asymptotically approaches to  $T_x/T_{total} = b_x = 44\%$  and  $59\%$  for the five-story model and the 17-story model, respectively, when values of  $e_y$  go to  $\pm$ infinity. It diverges to  $\pm$ infinity when  $T_{total}$  approaches to 0 at  $e_y = 0.74\%$  for the five-story model and at  $e_y = -12.7\%$  for the 17-story model. Dashed lines corresponding to  $\gamma = +2$  and  $-2$  in Fig. 15(d) cover the

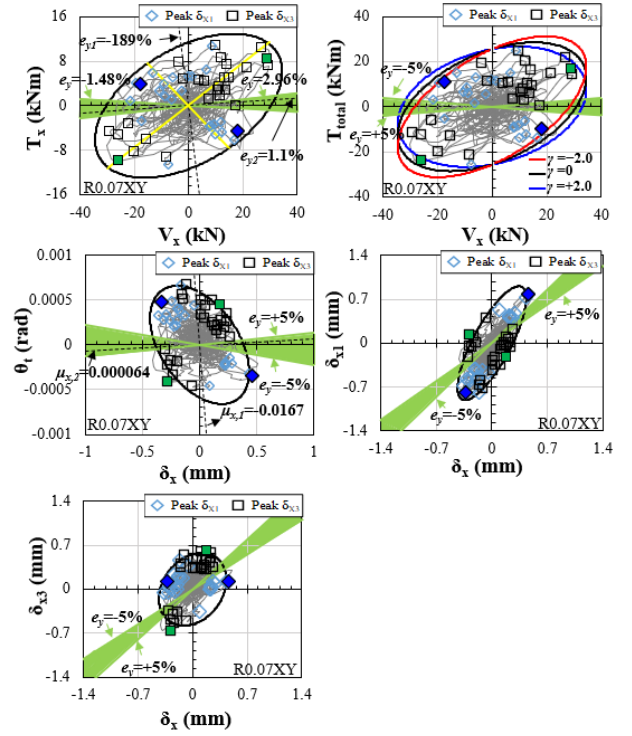


Fig. 16 Elliptical bounding of (a)  $T_x$ - $V_x$ ; (b)  $T_{total}$ - $V_x$ ; (c)  $\theta_t$ - $\delta_x$ ; (d)  $\delta_{x1}$ - $\delta_x$ ; and (e)  $\delta_{x3}$ - $\delta_x$  for the five-story model

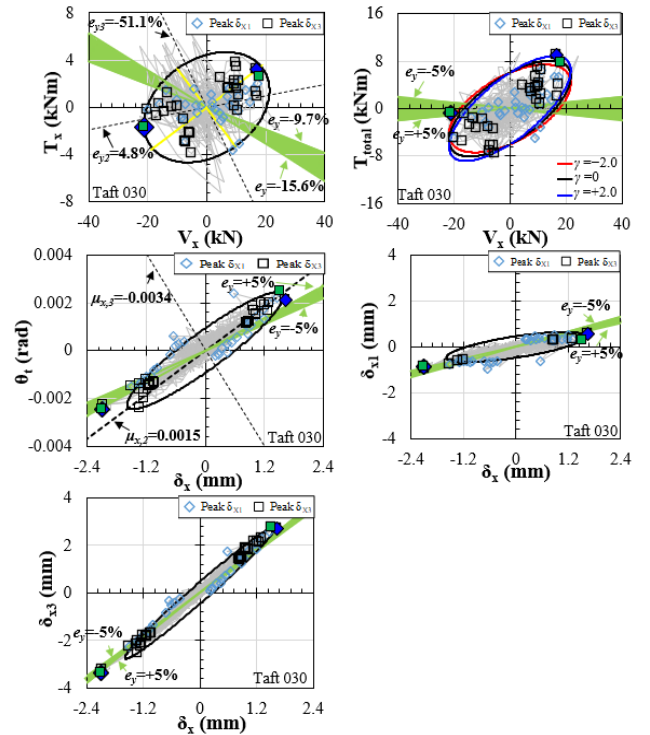


Fig. 17 Elliptical bounding of (a)  $T_x$ - $V_x$ ; (b)  $T_{total}$ - $V_x$ ; (c)  $\theta_t$ - $\delta_x$ ; (d)  $\delta_{x1}$ - $\delta_x$ ; and (e)  $\delta_{x3}$ - $\delta_x$  for the 17-story model

range of  $T_x/T_{total}$  in the experimental data fairly well. In summary, the dashed curves of Eqs. (8) - (12) in Fig. 15 are fairly consistent with data points from experimental results of five-story and 17-story models despite some scatters and outliers.

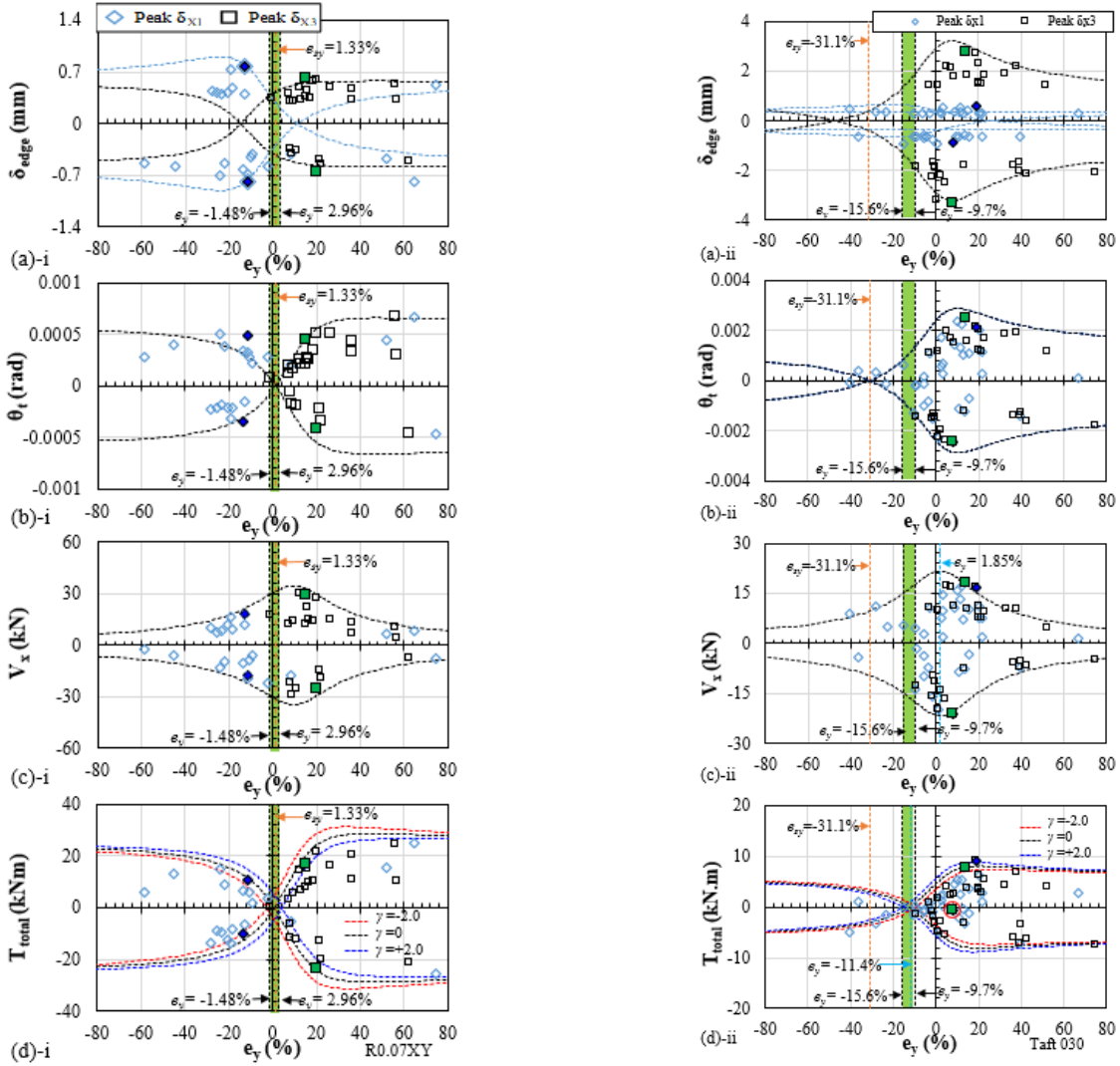


Fig. 18 Distributions of critical responses of (a)  $T_{total}/V_x$ ;  $T_x/V_x$ ;  $T_y/V_x$ ; (b)  $\delta_{edge}/\delta_x$ ; (c)  $\theta/\delta_x$ ; and (d)  $T_x/T_{total}$  at instants of peak  $\delta_{edge}$  compared to prediction equations for: i) the five-story and ii) the 17-story models

### 5.3 Use of ellipse for bounding responses at peak drifts

Because the behavior of the five-story model is governed by the combination of mode 1 and mode 2 in Fig. 14(a), the maximum point P1 is located on the major axis of the ellipsoid representing the half angle between the two modal eccentricities,  $e_{y1}$  and  $e_{y2}$ , with P2 located on the minor axis perpendicular to the major axis in Fig. 2(b). Similarly, because the 17-story model is predominantly governed by the second mode as shown in Fig. 14(b), the ellipse was constructed by assuming that P1 is tentatively located on the major axis of the second modal eccentricity,  $e_{y2}$ , in Fig. 2(c).

However, because of a small, but non-negligible contribution from the third mode, the ellipse with the major axis given by the second modal eccentricity does not represent the actual relationship between  $T_x$ - $V_x$ . Thus, the major axis was adjusted by trial and error, with P2 being located on the minor axis perpendicular to the adjusted major axis in Fig. 2(c).

Elliptical boundaries for the five-story model and the 17-story model have different overall shapes in Figs. 16 and 17. Especially, the ratio of the length of the major axis to that of the minor axis of the ellipse for the five-story model is 1.7 while that of the 17-story model is 3.8. The difference is because the two consecutive modes (first and second modes) have a combined contribution for the five-story model in contrast to the predominance of the second mode for the 17-story model. In Fig. 16(a), the maximum edge-frame drift points in  $T_x$ - $V_x$  of the five-story model denoted by green solid rectangles and blue solid diamonds are located along the major and minor axes of the ellipse, respectively, which lie between the two slopes representing modal eccentricities of the first mode and the second mode. The maximum  $\delta_{x3}$  represents the major axis while the maximum  $\delta_{x1}$  represents the minor axis of the ellipse. In Fig. 17(a), all maximum edge-frame drift points in  $T_x$ - $V_x$  of the 17-story model are near the slope of the eccentricity of the second mode,  $e_{y2} = 4.8\%$ , which is the predominant mode.

Grey peaks and valleys extruding outside the elliptical

Table 6 Values of drifts and forces at critical instants for the five-story model

	(a) Inherent torsion ( $T_{total}=0$ )	(b) X-dir. translation	Accidental torsion		(e) Rotation only	(f) $\delta_{x3,max}$	(g) $\delta_{x1,max}$
			(c) (-5%)	(d) (+5%)			
$e_y$ (%)	0.74	1.33	-1.48	2.96	490	46.8	-24.1
$\eta_y$ (%)	0	1.33	-5	5	1102	104	-47.7
$\delta_{x1}$ (mm)	0.443	-0.464	-0.354	0.533	-0.569	-0.114	0.908
$\delta_{x3}$ (mm)	0.478	-0.464	-0.510	0.433	0.569	0.579	-0.227
$\delta_x$ (mm)	0.460	-0.464	-0.432	0.483	0	0.233	0.340
$V_x$ (kN)	31.1	-31.3	-29.3	32.5	1.23	14.1	17.4
$T_x$ (kNm)	0.44	-0.790	0.82	1.83	11.4	12.5	-7.97
$T_{total}$ (kNm)	0	-0.790	2.78	3.08	25.7	28.6	-15.8
$\theta_t$ ( $\times 10^{-4}$ rad)	0.18	0	-0.82	-0.53	5.99	4.90	-5.97
$\delta_{edge}/\delta_x$	1.01	1	1.18	1.10	$\infty$	5.08	2.67

\* The value of  $T_{total}$  corresponds to  $\gamma = 0$

boundary in Fig. 17(a) are due to the raggedness of the time history of shear force in Frame X1 since it was determined by subtracting shear forces in frames X2 and X3 from the total inertial shear force which has noise in the time history (Ko and Lee 2006). As shown in Fig. 17, positive maximum values of  $\delta_{x1}$  and  $\delta_{x3}$  occur at instants close to each other whereas negative maximum values of  $\delta_{x1}$  and  $\delta_{x3}$  occur at the same instant.

The green region representing the range of the accidental torsion,  $\eta_y = T_{total}/V_x = -5\%$  to  $+5\%$  in Fig. 16(b) has a range of  $e_y = T_x/V_x = -1.48\%$  to  $+2.96\%$  for the five-story model in Fig. 16(a). However, the range of  $\eta_y = T_{total}/V_x = -5\%$  to  $+5\%$  in Fig. 17(b) has a range quite different from the corresponding range of  $e_y = T_x/V_x = -15.6\%$  to  $-9.7\%$  for the 17-story model shown in Fig. 17(a). This is because of the difference in the static eccentricity of  $e_{sy} = 1.33\%$  and  $e_{sy} = 31.6\%$  for the five-story model and the 17-story model, respectively. Both Figs. 16 and 17 show that the elliptical boundaries of  $T_{total}-V_x$  are not influenced significantly by the value of  $\gamma$ , which varies from -2, via 0 to +2, and that those of  $T_x-V_x$ ,  $\theta_t-\delta_x$ ,  $\delta_{x1}-\delta_x$  and  $\delta_{x3}-\delta_x$  are independent of  $\gamma$ .

Fig. 18 shows distributions of  $\delta_{x1}$ ,  $\delta_{x3}$ ,  $\theta_t$ ,  $V_x$ , and  $T_{total}$  at peak edge-frame drifts with respect to  $e_y$  for five-story and 17-story models. For the five-story model, ranges of seismic responses at the ground story are  $\delta_{x1} = -0.79 \sim 0.79$  mm,  $\delta_{x3} = -0.67 \sim 0.61$  mm,  $\theta_t = -0.00046 \sim 0.00066$  rad,  $V_x = -29.0 \sim 29.5$  kN, and  $T_{total} = -23.9 \sim 21.6$  kNm, with  $e_y$  ranging from -58.6% to 74.6%. Similarly, for the 17-story model, ranges of seismic responses are  $\delta_{x1} = -0.86 \sim 0.57$  mm,  $\delta_{x3} = -3.34 \sim 2.75$  mm,  $\theta_t = -0.00249 \sim 0.00247$  rad,  $V_x = -21.3 \sim 18.2$  kN, and  $T_{total} = -7.57 \sim 9.08$  kNm, with  $e_y$  ranging from -40.3% to 74.8%. The maximum and minimum responses in Fig. 18 occur with similar eccentricities of same signs for both five-story model and the 17-story model. Although the maximum value of  $\delta_{x1}$  is larger than that of  $\delta_{x3}$  for the five-story model in Fig. 18 (a)-i, the shear force and the torsional moment corresponding to the maximum  $\delta_{x3}$  are greater than those corresponding to the maximum  $\delta_{x1}$  in Figs. 18 (c)-i and (d)-i. This is due to larger lateral and torsional stiffness values of the first mode, that controls  $\delta_{x3}$ , than those of the second mode as shown in Fig. 14 (a).

Dashed curves of critical responses versus  $e_y$  in Fig. 18

are determined based on elliptical boundaries in Figs. 16 and 17. In Fig. 18(a), theoretical curves reasonably predict the maximum edge-frame drifts from experimental results for both five-story and 17-story models. When  $e_y$  goes to infinity, drifts at the edge frame asymptotically approach to a constant value. In Fig. 18(c), the trend of curves of  $V_x$  versus  $e_y$  creates a curved bell shape whereas that of  $T_{total}$  creates a shape of an hourglass with zero  $T_{total}$  as the neck in Fig 18(d). The maximum shear force and zero torsional moments (inherent torsion) occur at different eccentricities for both five-story and 17-story models in contrast to the simultaneity assumption in the static torsion design approach. The maximum edge-frame drifts do not increase infinitely but are bounded. They can be estimated using Eqs. (7) - (13). More details about this will be discussed in the following subsection.

#### 5.4 The significance of the proposed concepts

Relationships shown in Figs. 19(a), 19(b) and 19(c) define different states, (a) to (g), representing different responses of interest in the space of shear force and torsional moment or in the space of  $\delta_{center}$  and  $\delta_{edge}$  with the corresponding information in Table 6.

Instant (a) is the state of inherent torsion with the value of  $T_{total} = 0$ . Ratios of  $\delta_{stiff}/\delta_x$  and  $\delta_{flex}/\delta_x$  are equal to 1 at instant (b) when the structure experiences translational movement only. The range from instants (c) to (d) in Figs. 19(a), 19(b) and 19(c) represent the range of  $\eta_y = T_{total}/V_x = -5\%/+5\%$  corresponding to the accidental torsion in current design codes. At instant (e), only the rotational movement occurs without translational movements.  $\delta_{x3}$  and  $\delta_{x1}$  reach their maximum at instants (f) and (g) in Figs. 19(b) and (c), respectively. When  $\delta_{x3}$  reaches the maximum, the corresponding  $\delta_{x1}$  becomes small and vice versa. The range of the accidental torsion ( $\pm 5\%$ ) is very limited range. The maximum edge-frame drifts occur outside of this range.

Fig. 19(d) shows the detailed relationship between  $T_{total}/V_x$ ,  $T_y/V_x$  and  $T_x/V_x = e_y$  around the inherent torsion,  $T_{total} = 0$ , with the range of accidental torsion  $\eta_y = \pm 5\%$ . At the static eccentricity,  $e_y = e_{sy} = 1.33\%$ , all torsional resistances come from X-directional frames, i.e.,  $T_{total} = T_x$ . There is no torsional deformation,  $\delta_{edge}/\delta_x = 1.0$  in Fig.

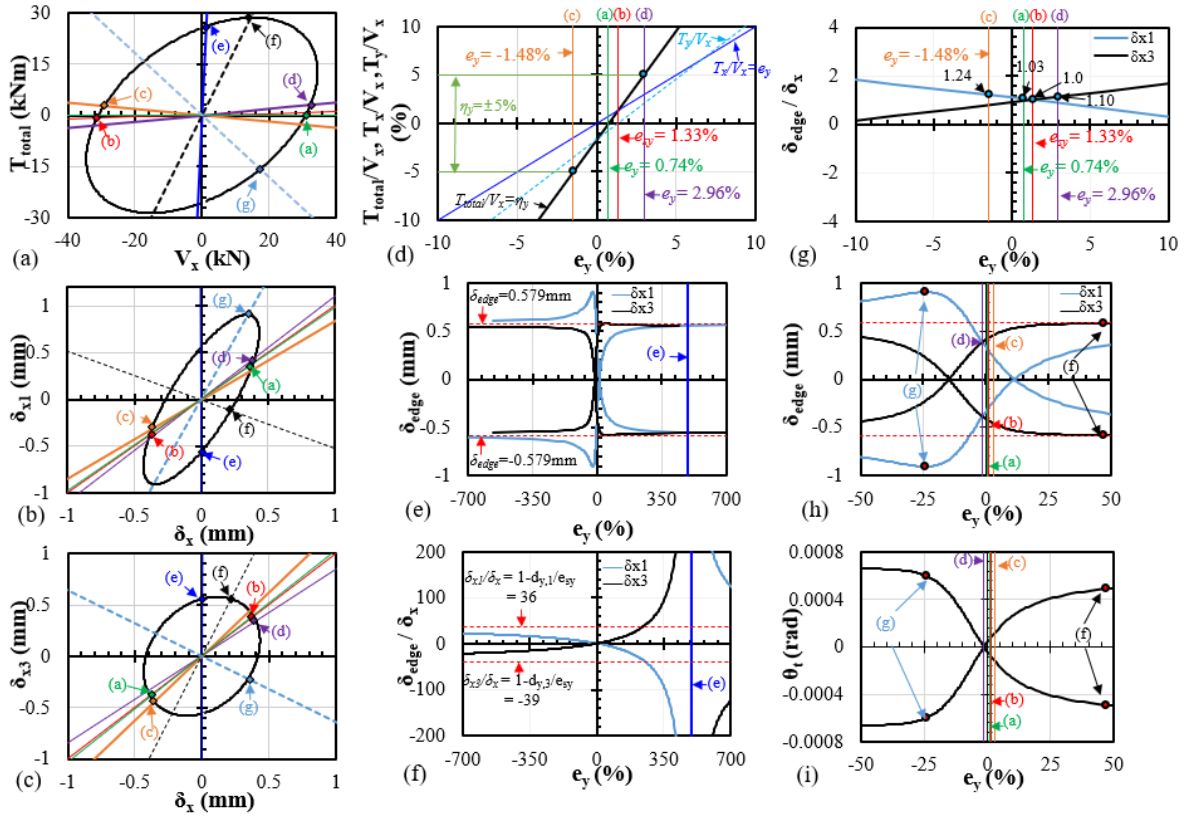


Fig. 19 Relationships of  $T_{total}/V_x$ ,  $T_x/V_x$ ,  $T_y/V_x$ ,  $\delta_{edge}$ ,  $\delta_{edge}/\delta_x$  and  $\theta_t$  versus  $e_y$  for five-story model

19(g). At the eccentricity corresponding to the inherent torsion,  $e_y=0.74\%$ , the torsional moment from X-directional frames,  $T_x$ , is equal to that from Y-directional frames,  $T_y$ , in the opposite direction, leading to zero  $T_{total}=T_x+T_y$ . However, at this inherent torsion, the  $\delta_{edge}/\delta_x$  becomes 1.03 (not 1.0). Over the range of  $\eta_y=-5\%$  to  $+5\%$  ( $e_y=-1.48\%$  to  $+2.96\%$ ), relations of  $T_x$ ,  $T_y$ , and  $T_{total}$  are shown in Fig. 19(d) with  $\delta_{edge}/\delta_x$  shown in Fig. 19(g).

The maximum edge-frame drifts of  $\delta_{x1}$  and  $\delta_{x3}$  are plotted as a function of the resistance eccentricity,  $e_y$ , in Figs. 19(e) and 19(h), where  $\delta_{x3}$  has the maximum drift of  $\pm 0.58$  mm at  $e_y=46.8\%$  denoted as (f) and  $\delta_{x1}$  has the maximum drift of  $\pm 0.91$ mm at  $e_y=-24.1\%$  denoted as (g) with all other related information given in Table 6. Fig. 19(e) shows not only the maximum drift, but also the overall distribution of the drift approaching to  $\delta_{x1}=\delta_{x3}=0.58$  mm at the  $\pm$ -infinite eccentricity.

Fig. 19(f) shows the trend of the ratio  $\delta_{edge}/\delta_x$  with the eccentricity. When the eccentricity increases to the negative infinity,  $\delta_{edge}/\delta_x$  asymptotically approaches to certain values,  $\delta_{x1}/\delta_x = 36$  and  $\delta_{x3}/\delta_x = -39$ .

However, when the eccentricity increases in the positive sense up to the state of rotational deformation only without translation movement which corresponds to instant (e) in Figs. 19(a), 19(b) and 19(c),  $\delta_{edge}/\delta_x$  approaches to  $\pm$  infinity at  $e_y = 490\%$ . Eccentricities corresponding to the maximum  $\delta_{x1}$  and the maximum  $\delta_{x3}$ ,  $-24.1\%$  and  $46.8\%$ , respectively, are quite outside of the range of  $e_y = -1.48\%$  to  $2.96\%$  corresponding to the accidental eccentricity,  $\eta_y=-5\%$  to  $+5\%$ , as shown in Figs. 19(h) and 19(i). Also, in Fig. 19(i),

torsional deformations at the maximum edge-frame drifts corresponding to instant (f) and instant (g) are substantially larger than those at the accidental torsion corresponding to instant (c) and instant (d).

By adopting the proposed two concepts, engineers not only can visualize the clear picture of the overall relationship between shear and torsion with the range of forces and deformations, but also can easily pinpoint the information about critical responses of structures such as the maximum and minimum edge-frame drifts and the corresponding shear force and torsion moment with the eccentricity.

### 5.5 Evaluation of validity of code static torsion design

The inherent torsion in the current code static eccentricity model represents a very specific instant of zero inertial torsional moment at the CM in contrast to the general state of the inertial torsion moment which can be very large in TU structures as shown in Fig. 19. Therefore, it is evident that the code static eccentricity model is not able to take the real torsional behavior of particularly TU structures into consideration. In Figs. 15-18, the range of accidental torsion eccentricity,  $\eta_a=T_{total}/V$  ( $-5\%$  to  $+5\%$ ), represented by the green region is very limited compared to the actual ranges of  $\eta_y$ ,  $-125\%$  to  $81\%$  for the five-story model and  $-60\%$  to  $100\%$  for the 17-story model, which correspond to the peak drift demands exceeding one-half of the maximum. The comparison of the green regions representing the accidental torsion with the overall range of

responses also clearly manifests why the accidental torsion causes only a negligible design impact despite the code-required cumbersome design procedure.

## 6. Conclusions

Current building codes require structures to be designed to be able to resist an elastic design torsional moment which includes the inherent torsional moment resulting from the static eccentricity,  $e_s$ , between the CM and the CR (CS) and the accidental torsional moment which considers many different types of uncertainty regarding torsion. The static torsion design procedure (see Fig. 1(a)) in these codes negates the possible existence of the inertial torsional moment,  $T_{total}$ , at the CM and only considers the accidental torsion at the CM.

The resistance eccentricity,  $e_y$ , commonly used by engineers as shown in Fig. 1(b) in FEMA 454 (2006), does not coincide with the  $e_s$  used for design eccentricity,  $e_d$ , in current codes.  $e_y$  is the distance between resultant inertial forces at the CM and the resultant resisting force of the structure in the specific direction of earthquake ground excitations as shown in Fig. 1(c). On the other hand,  $e_s$  and  $e_d = e_s \pm e_a$  in the code static eccentricity model are the rotational arm length of the inertial shear force at the CM with respect to the center of rotation, *i.e.*, the CS in Fig. 1(a). This discrepancy in the definition of eccentricity may lead to substantial confusion among engineers.

Using the resistance eccentricity model in Fig. 1(c), the following two concepts regarding the interaction between shear and torsion are proposed. First, for a general single-story two-way asymmetric structure, the story force  $\{V_x, V_y, T_{total}\}$  is related to the story drift  $\{\delta_x, \delta_y, \theta_i\}$  at the CM by Eq. (5) at instants of peak edge-frame drifts when the velocity is zero. That is, the resisting force by frames becomes equal to inertia forces in the dynamic equilibrium equation as given in Eq. (5).  $\eta_y = T_{total}/V_x$ ,  $\mu_x = \theta_i/\delta_x$ ,  $\delta_{edge}/\delta_x$  are given as a function of resistance eccentricity,  $e_y$ , in Eqs. (7) - (12). Secondly, hysteretic relationships between shear and torsion in forces and deformations are bounded by ellipsoids with corresponding major axes determined considering predominant modal eccentricities. Demands estimated using these two concepts are compared with demands from shake-table tests of two TU building structures under the SLE (a 1:5-scale five-story RC building model and a 1:12-scale 17-story RC building model) represented by the diamond markers and square markers in Fig. 13, which are selected only if the peak edge-frame drifts exceed one-half of the maximum positive and negative edge-frame drifts for the five-story and 17-story models.

The following conclusions are drawn from this study:

- The prediction of the critical torsional behavior by Eqs. (7) - (12) reveals the following characteristics:  $T_{total}/V_x$  is linearly proportional to  $e_y$  ( $= T_x/V_x$ );  $T_x/T_{total}$  approaches to a constant ratio when the absolute value of  $e_y$  is relatively large;  $T_x/T_{total}$  diverges to a positive or negative infinity value when  $T_{total}$  approaches to zero. Trends of data points,  $\delta_{edge}/\delta_x$  and  $\theta_i/\delta_x$ , at instants of

peak edge-frame drifts for the five-story model and the 17-story model under the SLE match the curves from prediction equations fairly well despite some scatters. These overall results prove that these prediction equations can serve as useful references for predictions of  $T_{total}/V_x$ ,  $T_x/T_{total}$ ,  $\delta_{edge}/\delta_x$ , and  $\theta_i/\delta_x$ .

- Instead of using any specific value of resistance eccentricity as a design parameter, seismic torsion demands are determined through a direct relationship with the base or story shear represented as an ellipse. These elliptical relationships bound actual experimental peak responses of the structure reasonably well. In particular, the hysteretic relationship between the drift at the edge frame with respect to the drift at the center of story can be conveniently visualized using an ellipsoidal model. However, further research is needed to elaborate methodologies in the construction of ellipsoidal boundaries.

- Concepts proposed in this study enable engineers to not only visualize the overall picture of torsional behavior including the relationship between shear and torsion with the range of forces and deformations, but also pinpoint easily the information about critical responses of structures such as the maximum and minimum edge-frame drifts and the corresponding shear force and torsion moment with the eccentricity.

- The inherent torsion in the current code static eccentricity model represents a very specific instant of zero inertial torsional moment at the CM in contrast to the general state of the inertial torsion moment which can be very large in TU structures. Therefore, it is evident that the code static eccentricity model is not able to take the real torsional behavior of particularly TU structures into consideration.

- The range of accidental torsion eccentricity,  $\eta_a = T_{total}/V$  (-5% to +5%) is very limited compared to the actual ranges of  $\eta_y$ , -125% to 81% for the five-story model and -60% to 100% for the 17-story model, which represent all the peak drift demands exceeding one-half of the maximum. The comparison of the range of responses representing the accidental torsion with the overall range of responses also clearly manifests why the accidental torsion causes only a negligible design impact despite the code-required cumbersome design procedure.

## Acknowledgments

The research was supported by grants (NRF-2009-0078771 and NRF-2017R1D1A1B03033488) of the National Research Foundation of Korea and a Korea University Grant. The authors are grateful for these supports.

## References

- AIK (2000), "Korean building code, KBC 2000", Architectural Institute of Korea, Seoul, Korea. (in Korean)  
 AIK (2005), "Korean building code, KBC2005", Architectural Institute of Korea, Seoul, Korea. (in Korean)

- Anagnostopoulos, S.A., Kyrkos, M.T. and Stathopoulos, K.G. (2015), "Earthquake induced torsion in buildings: critical review and state of the art", *Earthq. Struct.*, **8**(2), 305-377. <http://dx.doi.org/10.12989/eas.2015.8.2.305>.
- ASCE (2010), "*Minimum Design Loads for Buildings and Other Structures*", ASCE/SEI 7-10, *Ame. Soc. Civil Eng.*, Reston, V.A.
- Basu, D., Constantinou, M.C. and Whittaker, A.S. (2014), "An equivalent accidental eccentricity to account for the effects of torsional ground motion on structures", *Eng. Struct.*, **69**, 1-11. <https://doi.org/10.1016/j.engstruct.2014.02.038>.
- Chandler, A.M., Correnza, J.C. and Hutchinson, G.L. (1995), "Influence of accidental eccentricity on inelastic seismic torsional effects in building", *Eng. Struct.*, **17**(3), 167-178. [https://doi.org/10.1016/0141-0296\(94\)00003-C](https://doi.org/10.1016/0141-0296(94)00003-C).
- De la Llera, J.C. and Chopra, A.K. (1994a), "Evaluation of code accidental-torsion provisions from building records", *J. Struct. Eng.*, **120**(2), 597-616. [https://doi.org/10.1061/\(ASCE\)0733-9445\(1994\)120:2\(597\)](https://doi.org/10.1061/(ASCE)0733-9445(1994)120:2(597)).
- De la Llera, J.C. and Chopra, A.K. (1994b), "Accidental and natural torsion in earthquake response and design of buildings", EERC Report No. UCB/EERC-94/07; University of California, Berkeley, C.A, U.S.A.
- De la Llera, J.C. and Chopra, A.K. (1995), "Estimation of accidental torsion effects for seismic design of buildings", *J. Struct. Eng.*, **121**(1), 102-114. [https://doi.org/10.1061/\(ASCE\)0733-9445\(1995\)121:1\(102\)](https://doi.org/10.1061/(ASCE)0733-9445(1995)121:1(102)).
- DeBock, D.J., Liel, A.B., Haselton, C.B., Hooper, J.D. and Henige R.A. (2014), "Importance of seismic design accidental torsion requirements for building collapse capacity", *Earthq. Eng. Struct. Dyn.*, **43**(6), 831-850. <https://doi.org/10.1002/eqe.2375>
- FEMA 454 (2006), "*Designing for earthquakes—a manual for architects*", Federal Emergency Management Agency, Washington, DC.
- Humar, J.L. and Kumar, P. (1999), "Effect of orthogonal in plane structural elements on inelastic torsional response", *Earthq. Eng. Struct. Dyn.*, **28**(10), 1071-1097. [https://doi.org/10.1002/\(SICI\)1096-9845\(199910\)28:10](https://doi.org/10.1002/(SICI)1096-9845(199910)28:10).
- Hwang, K.R., Abegaz, R.A. and Lee, H.S. (2017), "Effects of torsional resistance by transverse frames on seismic drift demand of torsionally-unbalanced building structures", *The 2017 World Congress on Advances in Structural Engineering and Mechanics, ASEM17*, Ilsan (Seoul), Korea, August - September.
- KCI (2000), "*Design Code for Concrete Structures*", Korea Concrete Institute. (in Korean).
- Ko, D.W. and Lee, H.S. (2006), "Shaking table tests on a high-rise RC building model having torsional eccentricity in soft lower storeys", *Earthq. Eng. Struct. Dyn.*, **35**(11), 1425-1451. <https://doi.org/10.1002/eqe.590>
- Lam, N.T., Wilson, J.L. and Lumantarna, E. (2016), "Simplified elastic design checks for torsionally balanced and unbalanced low-medium rise buildings in lower seismicity regions", *Earthq. Struct.*, **11**(5), 741-777. <https://doi.org/10.12989/eas.2016.11.5.741>.
- Lee, H.S. and Hwang, K.R. (2015), "Torsion design implications from shake-table responses of an RC low-rise building model having irregularities at the ground story", *Earthq. Eng. Struct. Dyn.*, **44**(6):907-927. <https://doi.org/10.1002/eqe.2492>.
- Lee, H.S., Jung, D.W., Lee, K.B., Kim, H.C. and Lee K. (2011), "Shake-table responses of a low-rise RC building model having irregularities at first story", *Struct. Eng. Mech.*, **40**(4), 517-539. <https://doi.org/10.12989/sem.2011.40.4.517>
- Lee, H.S., Lee, K.B., Hwang, K.R. and Cho, C.S. (2013), "Shake-table responses of an RC low-rise building model strengthened with buckling restrained braces at ground story", *Earthq. Struct.*, **5**(6), 703-731. <https://doi.org/10.12989/eas.2013.5.6.703>.
- Lin, W.H., Chopra, A.K. and De la Llera, J.C. (2001), "Accidental torsion in buildings: analysis versus earthquake motions", *J. Struct. Eng.*, **127**(5), 475-481. [https://doi.org/10.1061/\(ASCE\)0733-9445\(2001\)127:5\(475\)](https://doi.org/10.1061/(ASCE)0733-9445(2001)127:5(475)).
- Lumantarna, E., Lam, N. and Wilson, J. (2018) "Methods of analysis for buildings with uni-axial and bi-axial asymmetry in regions of lower seismicity", *Earthq. Struct.*, **15**(1), 81-95. <https://doi.org/10.12989/eas.2018.15.1.081>.
- Paulay, T. (1998), "Torsional mechanisms in ductile building systems", *Earthq. Eng. Struct. Dyn.*, **27**(10), 1101-1121. [https://doi.org/10.1002/\(SICI\)1096-9845\(199810\)27:10](https://doi.org/10.1002/(SICI)1096-9845(199810)27:10).
- Stathopoulos, K.G. and Anagnostopoulos, S.A. (2010), "Accidental design eccentricity: Is it important for the inelastic response of buildings of buildings to strong earthquakes?", *Soil Dyn. Earthq. Eng.*, **30**(9), 782-797. <https://doi.org/10.1016/j.soildyn.2009.12.018>.
- UBC 97 (1997), Uniform Building Code, International Council of Building Officials (ICBO), Whittier, C.A.

CC

## Appendix

Derivation of prediction equations as a function of resistance eccentricity for a single-story two-way asymmetric-plan structure system

For a general single-story two-way asymmetric structural system, the story force vector  $\{V_x, V_y, T_{total}\}$  at the CM is related to the inter-story drift vector  $\{\delta_x, \delta_y, \theta_t\}$  at the CM as shown in Eq. (A1) (Eq. (5)) at instants of peak edge-frame drifts when the velocity becomes zero and, therefore, the resisting force by frames becomes equal to the inertia force in the dynamic equilibrium equation.

$$\begin{Bmatrix} V_x \\ V_y \\ T_{total} \end{Bmatrix} = \begin{bmatrix} K_X & 0 & K_{\theta X} \\ 0 & K_Y & K_{\theta Y} \\ K_{\theta X} & K_{\theta Y} & K_{\theta\theta} \end{bmatrix} \begin{Bmatrix} \delta_x \\ \delta_y \\ \theta_t \end{Bmatrix} \quad (\text{A1})$$

$$(5)$$

Using Eq. (A1) (Eq. (5)), the forces,  $V_x, V_y, T_{total}$ , at the CM can be expressed as follows:

$$K_X \delta_x + K_{\theta X} \theta_t = V_x \quad (\text{A2a})$$

$$K_Y \delta_y + K_{\theta Y} \theta_t = V_y \quad (\text{A2b})$$

$$K_{\theta X} \delta_x + K_{\theta Y} \delta_y + K_{\theta\theta} \theta_t = T_{total} \quad (\text{A2c})$$

$T_{total}$  in Eq. (A2c) can be rewritten as a sum of  $T_x$  and  $T_y$  as

$$\begin{aligned} T_{total} = T_x + T_y &= K_{\theta X} \delta_x + K_{\theta Y} \delta_y + (K_{\theta\theta X} + K_{\theta\theta Y}) \theta_t \\ &= \underbrace{K_{\theta X} \delta_x + K_{\theta\theta X} \theta_t}_{T_x} + \underbrace{K_{\theta Y} \delta_y + K_{\theta\theta Y} \theta_t}_{T_y} \end{aligned} \quad (\text{A3})$$

From Eq. (A1) (Eq. (5)), the displacements  $\delta_x, \delta_y$ , and  $\theta_t$  at the CM can be expressed as follows:

$$\delta_x = \frac{V_x - \theta_t K_{\theta X}}{K_X} \quad (\text{A4a})$$

$$(6-a)$$

$$\delta_y = \frac{V_y - \theta_t K_{\theta Y}}{K_Y} \quad (\text{A4b})$$

$$(6-b)$$

$$\theta_t = \frac{T_{total} - e_{sy} V_x - e_{sx} V_y}{K_{\theta s}} \quad (\text{A4c})$$

$$(6-c)$$

The resistance eccentricity,  $e_y = T_x/V_x$ , in Eq. (A5) (Eq. (7)) is determined by using Eq. (A2a) and Eq. (A3)

$$e_y = \frac{T_x}{V_x} = \frac{\delta_x K_{\theta X} + \theta_t K_{\theta\theta X}}{\delta_x K_X + \theta_t K_{\theta X}} \quad (\text{A5})$$

$$(7)$$

$\theta_t$  in Eqs. (A2a), (A2b) and (A2c) can be expressed as follows:

$$\theta_t = \frac{V_x - K_X \delta_x}{K_{\theta X}} \quad (\text{A6a})$$

$$\theta_t = \frac{V_x - K_Y \delta_y}{K_{\theta Y}} \quad (\text{A6b})$$

$$\theta_t = \frac{T_{total} - K_{\theta X} \delta_x - K_{\theta Y} \delta_y}{K_{\theta\theta}} \quad (\text{A6c})$$

$\delta_x$  can be represented in Eq. (A7) by substituting Eq. (A6a) into Eq. (A6b),

$$\delta_x = \frac{K_{\theta Y} V_x - K_{\theta X} V_y + K_Y K_{\theta X} \delta_y}{K_X K_{\theta Y}} \quad (\text{A7})$$

$\theta_t$  can be rewritten in Eq. (A8) by substituting Eq. (A7) into Eq. (A6c),

$$\begin{aligned} \theta_t &= \frac{T_{total} - K_{\theta X} \left( \frac{K_{\theta Y} V_x - K_{\theta X} V_y + K_Y K_{\theta X} \delta_y}{K_X K_{\theta Y}} \right)}{K_{\theta\theta}} \\ &= \frac{K_{\theta Y} \delta_y}{K_{\theta\theta}} \\ &= \frac{T_{total}}{K_{\theta\theta}} - \frac{K_{\theta X}}{K_X K_{\theta Y}} V_x \\ &\quad + \frac{K_{\theta X}^2 V_y - (K_Y K_{\theta X}^2 + K_X K_{\theta Y}^2) \delta_y}{K_X K_{\theta Y} K_{\theta\theta}} \end{aligned} \quad (\text{A8})$$

$\delta_x, \delta_y$  and  $\theta_t$  at the CM can be expressed using Eqs. (A6), (A7), and (A8) as follows:

$$\delta_x = \frac{T_{total} (K_Y K_{\theta X}) - K_{\theta X} K_{\theta Y} V_y + (K_{\theta Y}^2 - K_Y K_{\theta\theta}) V_x}{K_Y K_{\theta X}^2 + K_X K_{\theta Y}^2 - K_X K_Y K_{\theta\theta}} \quad (\text{A9a})$$

$$\delta_y = \frac{T_{total} (K_X K_{\theta Y}) - K_{\theta X} K_{\theta Y} V_x + (K_{\theta X}^2 - K_X K_{\theta\theta}) V_y}{K_Y K_{\theta X}^2 + K_X K_{\theta Y}^2 - K_X K_Y K_{\theta\theta}} \quad (\text{A9b})$$

$$\theta_t = \frac{T_{total} - e_{sy} V_x - e_{sx} V_y}{K_{\theta s}} \quad (\text{A9c})$$

$e_y$  in Eq. (A10) (Eq. (8)) can be obtained by substituting Eqs. (A9a) and (A9c) into Eq. (A5),

$$\begin{aligned} e_y &= \frac{K_{\theta X} \delta_x + K_{\theta\theta X} \theta_t}{K_X \delta_x + K_{\theta X} \theta_t} \\ &= \frac{(K_{\theta\theta X} - e_{sy}^2 K_X) \eta + (K_{\theta\theta Y} - e_{sx}^2 K_Y) e_{sy}}{K_{\theta\theta} - e_{sy}^2 K_X - e_{sx}^2 K_Y} \\ &\quad - \frac{(K_{\theta\theta X} - e_{sy}^2 K_X) e_{sx} \gamma}{K_{\theta\theta} - e_{sy}^2 K_X - e_{sx}^2 K_Y} \\ &\quad \left( \because \eta_y = \frac{T_{total}}{V_x} \text{ and } \gamma_y = \frac{V_y}{V_x} \right) \\ &= \frac{(K_{\theta SX}) \eta_y + (K_{\theta SY}) e_{sy} - (K_{\theta SX}) e_{sx} \gamma_y}{K_{\theta s}} \\ &\quad \left( \because b_x = \frac{K_{\theta SX}}{K_{\theta s}} \text{ and } b_y = \frac{K_{\theta SY}}{K_{\theta s}} \right) \\ &= b_y e_{sy} + b_x (\eta_y - e_{sx} \gamma_y) \end{aligned} \quad (\text{A10})$$

$$(8)$$

$\eta_y = T_{total}/V_x$  in Eq. (A11) (Eq. (9)) can be expressed with

respect to  $e_y$  using Eq. (A10) (Eq. (8))

$$\eta_y = \frac{e_y - b_y e_{sy}}{b_x} + e_{sx} \gamma_y \quad (\text{A11})$$

(9)

$\mu_x = \theta_t / \delta_x$  with respect to  $e_y$  in Eq. (A12) (Eq. (11)) can be derived by using Eqs. (A4a) (Eq. (6a)) and (A9c),

$$\begin{aligned} \mu_x &= \frac{\theta_t}{\delta_x} = \frac{\theta_t}{\frac{V_x - K_{\theta y} \theta_t}{K_x}} = \frac{K_x \theta_t}{V_x - e_{sy} K_x \theta_t} \\ &= \frac{(T_{total} - e_{sy} V_x - e_{sx} V_y) K_x}{K_{\theta S} V_x - (T_{total} - e_{sy} V_x - e_{sx} V_y) e_{sx} K_x} \\ &= \frac{(\eta_y - e_{sy} - \gamma_y e_{sx}) K_x}{K_{\theta S} - (\eta_y - e_{sy} - \gamma_y e_{sx}) e_{sy} K_x} \\ &\quad \left( \begin{aligned} \because \eta_y - e_{sy} - \gamma_y e_{sx} &= \frac{e_y - b_y e_{sy} - b_x e_{sx}}{b_x} \\ &= \frac{e_y - e_{sy}}{K_{\theta SX} / K_{\theta S}} \end{aligned} \right) \\ &= \frac{\left( \frac{e_y - e_{sy}}{K_{\theta SX} / K_{\theta S}} \right) K_x}{K_{\theta S} - \left( \frac{e_y - e_{sy}}{K_{\theta SX} / K_{\theta S}} \right) e_{sy} K_x} \\ &= \frac{(e_y - e_{sy}) K_x}{K_{\theta SX} - (e_y - e_{sy}) e_{sy} K_x} \\ &= \frac{e_y - e_{sy}}{(K_{\theta \theta X} / K_x) - e_y e_{sy}} \quad (\text{A12}) \\ &\quad \left( \because K_{\theta SX} = K_{\theta \theta X} - e_{sy}^2 K_x \right) \quad (11) \end{aligned}$$